Enhancing the accuracy of weather radar heavy rainfall estimates in mountainous regions using combined radar quality indices

Methaprayun, Monton; Bogaard, Thom; Mapiam, Punpim Puttaraksa

DOI
10.1016/j.jhydrol.2025.133907

Publication date
2025

Document Version
Final published version

Published in
Journal of Hydrology

Citation (APA)
Methaprayun, M., Bogaard, T., & Mapiam, P. P. (2025). Enhancing the accuracy of weather radar heavy rainfall estimates in mountainous regions using combined radar quality indices. *Journal of Hydrology*, *662*, Article 133907. https://doi.org/10.1016/j.jhydrol.2025.133907

Journal of Hydrology 662 (2025) 133907

Contents lists available at ScienceDirect

Journal of Hydrology

journal homepage: www.elsevier.com/locate/jhydrol

Research papers

Enhancing the accuracy of weather radar heavy rainfall estimates in mountainous regions using combined radar quality indices

Monton Methaprayun [a], Thom Bogaard [b,a], Punpim Puttaraksa Mapiam [a,*]

[a] Department of Water Resources Engineering, Kasetsart University, PO Box 1032, Bangkok 10900, Thailand
[b] Department of Water Management, Delft University of Technology, PO Box 5048, 2600 GA Delft, The Netherlands

ARTICLE INFO

This manuscript was handled by Marco Borga, Editor-in-Chief, with the assistance of Francesco Marra, Associate Editor

Keywords:
Composite radar rainfall
Radar quality index
Beam blockage
Bias adjustment
Mountainous region
Thailand

ABSTRACT

With the availability of an increased number of ground-based weather radars, the development of composite radar rainfall estimates has become common practice. In mountainous terrain, weather radar measurements often encounter beam blockage effects, resulting in erroneous estimates of rainfall. This study introduces a novel relative radar quality index based on the radar reflectivity fraction to enhance the radar composite product. Additionally, we develop an improved mean field bias adjustment technique by including the spatial variability of the bias adjustment factors associated with the quality of radar observations. Radar reflectivity data from a network of single-polarization S-band radars, the Sattahip and Phimai radar stations in Thailand, and automatic rain gauges within the composite area, were used for the analysis. Three independent datasets were employed: (1) 51 storm events (2016–2022) for evaluating radar composite performance and QI-based bias adjustment; (2) hourly data from August–October 2020 to assess bias factor uncertainty; and (3) three heavy storms (2016, 2017, and 2020) to examine the QI method's effectiveness in beam-blocked basins. Our analysis explored seven combinations of hourly radar composite products. Subsequently, the performance of radar rainfall estimates obtained from applying the proposed mean field bias was evaluated by comparing them with the conventional technique. Results show the potential of integrating combined multiple quality indices to improve rainfall estimates, particularly for heavy rainfall events in mountainous regions.

1. Introduction

Spatio-temporal variation in rainfall and specific catchment characteristics strongly influence the hydrological and geomorphological behaviour of catchments. Especially, mountain regions have complex topography, climate patterns, and consequently meteorological conditions, which pose challenges for predicting heavy rainfall and consequently flash floods and landslides (Creutin and Borga, 2003; Guzzetti et al., 2007; Bogaard and Greco, 2018). In Thailand, local heavy rainfall typically coincides with weather conditions such as the monsoon, monsoon trough, low-pressure cell, and tropical cyclones. Tracking heavy storms in mountain regions is a challenging task that requires reliable and accurate data with high spatial and temporal resolution. Using only ground-based rain gauge monitoring networks with their notorious low density may not capture the high spatial and temporal rainfall variability, reducing the effectiveness of real-time early warning systems (Mekonnen et al., 2021; Overeem et al., 2023).

Integrating data from weather radars and rain gauge networks has been recognized as a promising way to obtain reliable rainfall products and is commonly used for high-resolution rainfall estimates at catchment scales (Smith and Krajewski, 1991; Cole and Moore, 2008; Mapiam et al., 2022; Mapiam et al., 2023). Weather radars can scan large areas and capture the spatiotemporal distribution of rainfall fields better than rain gauge networks. Radar-derived rainfall estimates are becoming ever more essential for a range of applications such storm tracking, flood prediction and landslide forecasting. However, being a ground-based remote sensing technique, weather radar is an indirect rainfall measurement technology that could be inaccurate, notably for extreme rainfall magnitudes (Bárdossy and Pegram, 2017; Marra and Morin, 2015; Schleiss et al., 2020). Consequently, correcting for multiple sources of error while generating radar rainfall products is a crucial procedure to improve the accuracy of radar rainfall estimates (Harrison et al., 2009; Krajewski et al., 2010; Villarini and Krajewski, 2010).

Mountainous terrain is known to present distinct challenges for weather radar measurements. Positioning a radar station in areas characterized by large elevation differences unavoidably leads to beam

* Corresponding author.
E-mail address: punpim.m@ku.th (P.P. Mapiam).

https://doi.org/10.1016/j.jhydrol.2025.133907
Received 28 February 2025; Received in revised form 5 July 2025; Accepted 12 July 2025
Available online 17 July 2025

blockage and ground clutter effects (Joss et al., 1990). Relying on data from a single weather radar might result in an underestimation of rainfall due to the beam blockage effect (Kucera et al., 2004). This issue is linked to the concept of hydrologic visibility, which refers to the ability of a weather radar to detect and provide accurate rainfall data across a given area, influenced by topographic features that obstruct radar signals (Pellarin et al., 2002). Traditionally, the digital elevation model (DEM) and radar beam characteristics are used to identify topographic regions with beam blockage (Krajewski et al., 2006; Lang et al., 2009). The blocked regions experience reduced radar visibility, resulting in inaccurate rainfall estimates that can negatively impact hydrologic modeling and decision-making processes. When only a single weather radar is available, rainfall estimates affected by partial beam blockage can be corrected with values derived from adjacent unblocked area estimates or using a multiplicative correction factor (Bech et al., 2007; McRoberts and Nielsen-Gammon, 2017). However, in the case where the radar signal is significantly obscured, this issue can be mitigated through radar compositing techniques utilizing data from multiple radar networks (Méri et al., 2021).

In practice, weather radars are situated as such that they have overlapping coverage. Logically, many studies have taken advantage of these radar networks to enhance data accuracy in regions with overlapping measurements using radar composite techniques (Holleman, 2007; Einfalt and Lobbrecht, 2012; Antonini et al., 2017). Conventionally, the composite estimate algorithm is straightforward by selecting the maximum value of the available reflectivity (MAX) at the pixel. However, this approach does not ensure a quality-proof composite product. It has an inherent tendency to overestimate if they are unbiased, and it can propagate non-meteorological echoes from individual radars (Fornasiero et al., 2006; Jurczyk et al., 2020).

Prior studies have introduced more sophisticated compositing methodologies by taking into account the quality of the radar measurements, usually characterized using quality information or quality indices (QIs) for each radar station (Saltikoff et al., 2019; Méri et al., 2021; Ośródka and Szturc, 2022). Various factors affecting the quality of radar measurement can be classified into two primary domains. The first group originates from the radar hardware and the settings of the measurement parameters (e.g., the power, wavelength, beamwidth, pulse length, and detection range). The second domain is influenced by the surrounding environment (e.g., the distance from the radar site, the altitude of the radar beam above the ground, beam blockage, sea clutter, and interference with other electronic devices). While various quality factors can be used, the distance from the radar or the beam height is most frequently taken as the main quality factor for simplicity (Jurczyk et al., 2020; Méri et al., 2021). Different QIs have been proposed, representing a range of factors affecting radar data and its quality. For example, the distance QI expresses the decrease of the quality of the radar signal as function of its distance from the radar source. In comparison, the beam height QI designates that the closer the radar beam is to the land surface, the more accurate the rainfall estimation is. Understandably, integrating multiple quality indices for composite computation has been introduced to enhance effectiveness. The overall quality indices of each radar station are generally derived from the multiplicative combination of a set of representative quality factors. In mountainous areas, the expected beam blockage is the key quality factor commonly employed to calculate the overall QI (Crisologo et al., 2018; Zhang et al., 2022). The value of the radar reflectivity in an overlapping area is computed as a QI-weighted average from the available radars at the specified pixel. For radar-based rainfall estimation, the generated composite reflectivity is subsequently transformed using the *Z-R* relationship. It is crucial to underline that the major sources of uncertainty consists of the variability in the vertical profile of reflectivity (VPR) (Hazenberg et al., 2013), the reflectivity measurement itself, the error caused by the attenuation effect (Hitschfeld and Bordan, 1954; Uijlenhoet and Berne, 2008), and the conversion to rainfall depth (*Z-R* conversion) (Uijlenhoet, 2001). Hereto, the Mean Field Bias (MFB) is an effective correction technique to reduce the residual errors between radar rainfall estimates and rain gauge data caused by these sources of error (Smith and Krajewski, 1991; Thorndahl et al., 2014; Schleiss et al., 2020; Imhoff et al., 2021).

Most previous studies have proposed quality indices based on the surrounding environment of an individual radar. Therefore, the calculated overall QI is helpful to assess the spatial reliability of the reflectivity measurement within a specified radar coverage having uniform radar system characteristics. Unfortunately, when using multiple radar scans with different hardware properties, it includes variations in the overall quality of each contributing radar (Krajewski et al., 2017; Keem et al., 2019). This typically results in diverse reflectivity data for each individual radar. Hence, it becomes imperative to introduce an additional Quality Index that reflects the degree of the relative quality of individual radars within the composite region. Moreover, after the compositing process, an effective bias correction technique is imperative for enhancing the quality of radar rainfall estimates. The MFB adjustment is the conventional method to obtain a static bias factor that is homogeneous in space but varies in time. The MFB approach neglects the uncertainty associated with the quality of radar observations, nor does it consider the spatial variability in bias factor (Seo et al., 1999; Michelson and Koistinen, 2000; Imhoff et al., 2021). This can lead to large errors in radar rainfall estimates, particularly in areas where the radar signal experiences blockage. The question that arises in this study is how radar data quality variations per station impact the spatial uncertainty of the mean field bias correction factor, especially in the beam blockage area.

This study aims to improve the accuracy of heavy rainfall estimates in mountainous areas using composite ground radar reflectivity information. Hereto, this study proposes a novel relative radar quality index scheme based on radar reflectivity fraction of the compositing radars. Moreover, we apply the relative radar quality indices to improve the mean field bias adjustment for radar derived rainfall estimates. Our study was founded in the overarching project to develop a near real-time flash flood and landslide early warning system using near real-time and nowcasted weather radar information as meteorological forcing. Therefore, as a case study, we applied our methodology on radar reflectivity data obtained from two weather radars over the mountainous area in northeastern Thailand, which is prone to severe hydrometeorological hazards. We show the level of improvement that is reached using the novel quality index scheme.

2. Theoretical framework: description of novel relative quality index and bias correction

2.1. Relative quality index

An effective radar composite method should retain all reliable measurement data while mitigating or at least minimizing the impact of lower-quality information (Jurczyk et al., 2020). This process of composite rain radar images is thought to reduce errors in the data obtained from individual radar stations and increase the accuracy of rainfall estimates. Hereto, the factors influencing the radar quality should be known a priori. The traditional compositing methods with a single quality factor are described below.

Operational systems traditionally use the Maximum and Mean methods for compositing radar reflectivity images. These approaches select either the maximum or mean values from the available reflectivity data collected by the relevant radar stations within the overlapping area. The Maximum method is known to mitigate common radar errors, such as attenuation in heavy rain and beam blockage, making it particularly popular for assessing high-intensity rainfall. However, this method is also known to overestimate radar composite values (Fornasiero et al., 2006; Holleman, 2007). On the other hand, the Mean method is typically effective when the radar data from each station shows relatively consistent reliability. It tends to underestimate reflectivities in the

composited area, though it has the advantage of mitigating non-meteorological echoes. A significant limitation of both techniques is its equal weighting of data, irrespective of whether it is proximate or distant from the radar. To evaluate the performance of conventional composite techniques in the Thai context, this study tested the Maximum method, which is widely used for heavy rainfall estimation. The analysis utilized 2.5-km pseudo-CAPPI (Constant Altitude Plan Position Indicator) reflectivity data from the Sattahip and Phimai radar stations to construct the radar composite.

More advanced compositing methodologies incorporate data quality considerations into their calculations. The most used single quality factor takes into account the distance from the radar (Fornasiero et al., 2006). This method calculates radar composite values prioritizing data from the radar station nearest to the specified area. This method aims to minimize errors obtained from data collected at greater distances, but a drawback of this method is the presence of discontinuities at the boundaries of radar coverage, stemming from different radar calibrations (Jurczyk et al. 2020, Barbieri et al. 2022). In an effort to enhance the accuracy of the radar composite product in mountainous areas, we calculate a composite quality index taking into account not only the distance from the radar station (QI_D), but also the height of the beam above the ground (QI_H) (Tabary, 2007) and the beam blockage fraction (QI_B) (Bech et al., 2003) quality indices (see Table 1). These radar quality indices are used to calculate the spatial overall quality indices for each radar station by multiplicative combination of relevant environmental quality factors. In the final step of radar compositing that we propose, the radar reflectivity value in an overlapping area is computed as a QI-weighted average of the available radars at the specified pixel.

To reduce the compositing errors caused by discrepancies in reflectivity data from multiple radar scans, we further incorporate the radar reflectivity fraction (QI_F) of the compositing radars. The QI_F is computed at the pixel level, representing the proportion of reflectivity from each radar relative to the total reflectivity from all radars involved in the compositing process (Eq. (1)). The QI_F is then combined with the environmental quality indices, QI_D, QI_H, and QI_B, for each radar to enhance the accuracy and representativeness of the final composited reflectivity field.

$$QI_{F_{i,j}} = \begin{cases} \dfrac{Z_{i,j}}{\sum_{i=1}^{N} Z_{i,j}}; \sum_{i=1}^{N} Z_{i,j} > 15\ dBZ \\ 1.0;\ \textit{No reflectivity returns} \end{cases} \quad (1)$$

where $Z_{i,j}$ is the measured radar reflectivity of radar station i at the specified radar pixel j, N is the total number of radar stations with overlapping measurement pixels used in the analysis. The resulting QI_F varies both spatially and temporally corresponding to the radar measurements.

Following the assessment of each QI at individual radar station, the subsequent step involves calculating the overall QI for each radar station. This process ultimately leads to the production of composite radar rainfall index. Operationally, the implementation proceeds as follows:

1. The initial step included generating three spatially varying quality indices (QI_D, QI_H, and QI_B) related to the surrounding environment
2. The collected instantaneous reflectivity data were applied to compute the spatio-temporally varying QI_F with a time scale corresponding to the resolution of measurement data.
3. Calculate the overall QI for each radar station by multiplying all four quality indices values together.

$$QI_{i,j} = QI_{D_{i,j}} \times QI_{H_{i,j}} \times QI_{B_{i,j}} \times QI_{F_{i,j}} \quad (2)$$

where $QI_{i,j}$ is the overall quality index for radar station i at pixel j.

2.2. Combining radar quality index with the bias correction

The implementation of an effective bias correction technique is essential for improving the accuracy of radar compositing, particularly in real-time operations (Steiner et al., 1999; Mapiam et al., 2022; Mapiam et al., 2023). However, using all radar-rain gauge pairs without filtering out poor-quality data can degrade the performance of quantitative precipitation estimation (QPE) (Zhang et al., 2022). Evaluating whether integrating the radar quality index can improve the mean field bias correction, especially in areas affected by signal blockage or low-quality regions, remains a challenging task.

Mean field bias (MFB) adjustment is a traditional and well-known technique aimed at deriving a static bias factor under the assumption that the Z-R relationship is homogeneous in space but exhibits variations over time. In this method, a multiplicative correction factor can be computed as the ratio of the mean hourly radar rainfall estimate to the rain gauge measurement (Yoo et al., 2014; Shi et al., 2018). The conventional analysis utilizes all rain gauges and radar data at the corresponding location to calculate a single correction factor across the entire radar area, without accounting for the uncertainty associated with the quality of radar observations or considering the spatial variability in the bias factor. However, the reliability of the observed radar data spatially changes over the radar coverage, leading to high variation in the observation bias factor, especially in areas where the radar reflectivity data was contaminated by various sources of measurement errors.

In this research, it is postulated that radar pixels with differing data quality should have different bias correction values. The computed QIs

Table 1
List of the three radar quality indices (QI_D, QI_H, and QI_B) related to the surrounding environment used in this study.

Quality Index	Equation	Condition of calculation	Parameters specification	References
1. QI_D	$QI_D = 1.0 - \frac{r - r_{min}}{r_{max} - r_{min}}$	$r_{min} \le r \le r_{max}$	Where r is the distance from the radar (km), r_{min} and r_{max} is the minimum and maximum distance from radar station. The $r_{min} = 0$ and $r_{max} = 240$ km for both Sattahip and Phimai radars.	Szturc et al. (2011)
2. QI_H	$QI_H = 1.0 - \frac{h}{h_{max}}$	$0 \le h \le h_{max}$	Where h is the bin height above terrain (km) and h_{max} is the maximum height above terrain of radar (km). The h_{max} for the Sattahip and Phimai radar were 5.65, and 6.93 km, respectively.	Tabary (2007)
3. QI_B	$QI_B = 1 - B$ $B = \frac{y\sqrt{a^2 - y^2} + a^2 \arcsin\left(\frac{y}{a}\right) + \frac{\pi a^2}{2}}{\pi a^2}$	$B \le B_{max}$	Where B (ranging between 0–1) is the proportion of radar beam obstructed by the terrain calculated based on the distribution of energy throughout the radar beam, and B_{max} is the maximum threshold of blockage which was set at 1 for the two radars. While a is the radius of the radar beam cross section, y is the difference between the center of radar beam and the topography. Note: When B-values are large, radar data becomes almost completely unreliable. Investigating the sensitivity of the B-value threshold used to define the QI_B factor is a relevant and beneficial issue for further analysis, particularly for composite regions where severe beam blockage affects a significant portion of the radar coverage. It is recommended that B values exceeding the defined threshold be assigned a QI_B value of zero.	Bech et al. (2003)

were used as indicators to distinguish radar data locations into different quality categories, and the bias adjustment factors associated with each category were afterwards determined independently. The overall QI of the radar composite using the quality index approach can be estimated using a probabilistic approach, as proposed by Méri et al. (2021) in Eq. (3). It is determined by subtracting the probability of an inaccurate measurement for the resulting product at a given pixel (P') from 1.0. The value of P' is obtained by multiplying the probability of poor measurements for each individual radar (P'_i). Each P'_i is then computed as 1.0 minus the multiplicative form of the overall QI for the corresponding radar station, as shown in Eq. (4). This overall QI of the radar composite will serve as a threshold for classifying radar quality:

$$\mathrm{QI}_{overall,j} = 1 - P' \tag{3}$$

$$P' = \prod_{i=1}^{N} P'_i = \prod_{i=1}^{N} (1 - \mathrm{QI}_{i,j}) \tag{4}$$

The overall QI of the radar composite will range from 0 to 1 and can vary both spatially and temporally due to various factors. Classifying QI values into multiple categories is a logical and challenging approach that may enhance the resolution of mean field bias (MFB) adjustments. However, uncertainties in radar and rain gauge observations can change dynamically. When the number of radar–gauge data pairs within each QI group is limited, the resulting MFB factors may be highly uncertain, potentially introducing large errors into the radar rainfall estimates (Thorndahl et al., 2014; Wright et al., 2014; Chen et al., 2019). To mitigate this issue, a two-group classification scheme was adopted in this study.

The bias correction method developed in this study was designed for near real-time operations in Thailand, where rainfall characteristics can vary substantially at sub-hourly timescales due to rapidly evolving storm systems, particularly during the monsoon season and tropical cyclones. Hourly bias adjustment is essential for capturing storm dynamics and improving the timeliness and accuracy of radar rainfall estimates (Wright et al., 2013; Mapiam et al., 2022). Although hourly bias factors are inherently more uncertain than those derived from longer periods (Thorndahl et al., 2014), applying MFB correction at finer temporal resolutions yields substantial improvements in rainfall estimates during extreme events (Wright et al., 2013; Mapiam et al., 2023). Accordingly, this study implemented bias adjustment at the hourly scale.

For each hour time step of the calculation, the process begins by spatially classifying radar pixels into two groups: 1) the group with radar data of high quality (QI above the threshold) and 2) the group with radar data of low quality (QI below the threshold). Subsequently, the MFB analysis is separately performed for each group using all radar-rain gauge pairs located in their group for calculation. The proposed mean field bias adjustment based on QI specifications at time t (MFB_{QI_t}) is illustrated by:

$$MFB_{\mathrm{QI}_t} = \begin{cases} \dfrac{\sum_{a=1}^{N_a} G_{a(high_{\mathrm{QI}}),t}}{\sum_{a=1}^{N_a} R_{a(high_{\mathrm{QI}}),t}}; \ if\ \mathrm{QI_a} \geq threshold \\ \dfrac{\sum_{b=1}^{N-N_a} G_{b(low_{\mathrm{QI}}),t}}{\sum_{b=1}^{N-N_a} R_{b(low_{\mathrm{QI}}),t}}; \ if\ \mathrm{QI_b} < threshold \end{cases} \tag{5}$$

where *threshold* is the defined threshold for classifying mean field bias into two groups, $R_{a(high_{\mathrm{QI}}),t}$ = the radar rainfall accumulation (mm) at the pixel corresponding to the a^{th} rain gauge with high QI for hour t, $G_{a(high_{\mathrm{QI}}),t}$ = the gauge rainfall data (mm) at gauge a for hour t, $R_{b(high_{\mathrm{QI}}),t}$ = the radar rainfall accumulation (mm) at the pixel corresponding to the b^{th} rain gauge with low QI for hour t, $G_{b(high_{\mathrm{QI}}),t}$ = the gauge rainfall data (mm) at gauge b for hour t, N = total number of rain gauges in the analysis, N_a = the total number of rain gauges with high QI. The optimal threshold has to be found empirically per study area. In this analysis, various QI thresholds were identified to calculate the QI-based MFB. The optimal threshold was selected based on the RMSE between adjusted radar rainfall estimates and corresponding rain gauge observations. For the radar rainfall correction process, the Z–R relationship proposed by Marshall and Palmer (1948) was used in combination with various configurations of QI factors to derive the initial composite radar rainfall. The QI-based bias adjustment was subsequently evaluated and applied as a multiplicative factor to correct the composited rainfall product. Further details on analysis of combined QI factors for radar rainfall compositing and the QI-based bias adjustment are provided in Section 4.1 and 4.2, respectively.

3. Description of study area and data availability

In this study, radar reflectivity data obtained from Sattahip and Phimai radars located in Chonburi (12.649° N, 100.963° E) and Nakhon Ratchasima (15.182° N, 102.564° E) provinces were used to construct the radar composite over the mountainous area in northeastern Thailand (Fig. 1). Both radars, operated by the Department of Royal Rainmaking and Agricultural Aviation (DRRAA), are single polarization S-band Doppler radars; however, they differ in several technical specifications, as summarized in Table A1. The DRRAA collected radar reflectivity data as volume scans at multiple elevation angles, with 14 angles for the Sattahip and 13 angles for the Phimai. The radar reflectivity product, provided in the form of pseudo-CAPPI, was delivered on a Cartesian grid covering 240 × 240 km^2, with a spatial resolution of 0.6 × 0.6 km^2 and a temporal resolution of 6 min. The pseudo-CAPPI was derived from the 2.5 km Constant Altitude Plan Position Indicator (CAPPI) and Plan Position Indicator (PPI) products. For each radar pixel within a radar range of 139 km for the Sattahip radar and 136 km for the Phimai radar, reflectivity values were taken from the elevation angle whose beam center was closest to 2.5 km altitude. Beyond these ranges, where all beam centers are above 2.5 km, reflectivity values were instead taken from the lowest elevation PPI (0.5°) for both radars.

Table A1 indicates that the Sattahip and Phimai radars have different hardware characteristics. The degradation of radar hardware over time can lead to calibration errors, which are a major source of uncertainty in radar measurements. In regions with similar climate and geography, differences in reflectivity measurements between radars are most likely attributable to calibration mismatches (Seo et al., 2014; Zhong et al., 2017, Warren et al., 2018; Keem et al., 2019). A comparison of radar reflectivity data within equidistant zones (Keem et al., 2019) of both radars, presented in Appendix A and Fig. A1, shows that the Sattahip radar consistently reports higher reflectivity values than the Phimai radar. This finding confirms that hardware performance plays a significant role in the observed discrepancies between the two datasets. Although achieving weather radar calibration is technically challenging, it is essential for ensuring data accuracy. Several calibration methods have been proposed. One common approach involves routine calibration using a metal sphere target, allowing for comparisons between measured and theoretical reflectivity values, with discrepancies used to adjust radar settings (Atlas, 2002). Additionally, intercomparisons of reflectivity data from ground-based radar networks or space-borne radar systems provide an effective means for monitoring and correcting calibration errors in operational radar systems (Keem et al., 2019; Lee et al., 2021). While these methods can lead to reasonably well-calibrated radar data, they typically require access to raw radar volume scans and operational hardware settings. In this study, the reflectivity data were provided by the DRRAA, and direct access to radar hardware or its calibration parameters was not available, as is recurrently the case in hydrological practice. As a result, analyzing radar composites without accounting for hardware-related discrepancies could lead to substantial errors in rainfall estimation. To mitigate this limitation, we applied the spatio-temporal radar reflectivity fraction ($\mathrm{QI_F}$), which represents the relative quality of individual radars within the overlapping region in the radar compositing process.

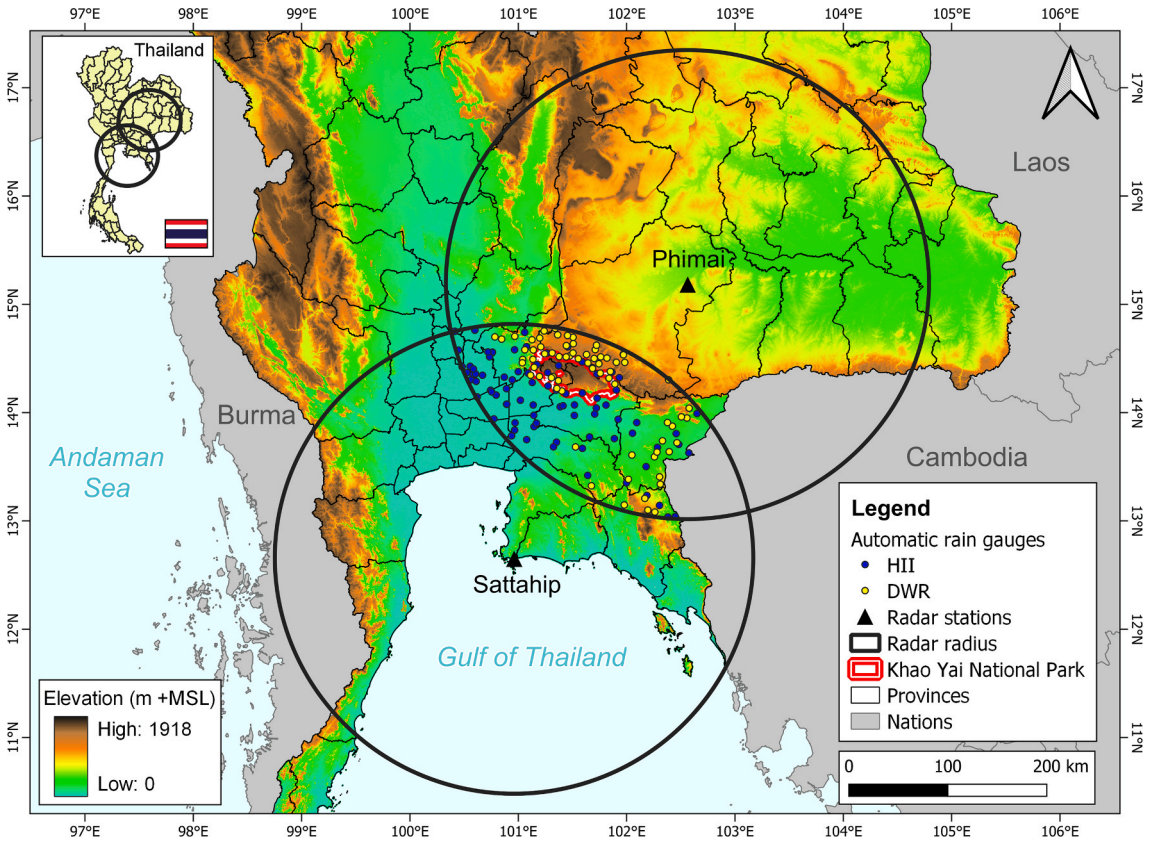

Fig. 1. Locations of the Sattahip and Phimai radars (with 240 km range markers) and the network of automatic rain gauges in the overlapping radar composite area.

The effect of ground clutter was filtered out from the radar data in this study by identifying clutter-prone areas characterized by persistently high reflectivity values, removing these areas from the radar map, and replacing them with interpolated values from surrounding pixels unaffected by clutter. Since S-band reflectivity data were used in this study, beam attenuation was generally assumed to be negligible (Hitschfeld and Bordan 1954; Delrieu et al. 2000). Nonetheless, the effect of attenuation was further investigated and confirmed to be insignificant for the S-band radar, as shown in Fig. A2 in Appendix A. The bright band effect on measured radar reflectivity was also investigated, as detailed in Fig. A3 in Appendix A, using an objective identification method proposed by Cheng and Collier (1993). The results suggest that the influence of measurement errors due to the bright band effect is negligible.

In analyzing the noise characteristics of the radar data, we found that the noise primarily consisted of low-intensity echoes scattered across the radar domain in patterns unassociated with precipitation. This phenomenon occurs dynamically and is more prevalent in tropical regions (Mesnard and Sauvageot, 2010). Several studies have recommended applying a 15 dBZ threshold to effectively remove such non-precipitating noise (Doviak and Zrnić, 1993; Dufton and Collier, 2015; Mapiam et al., 2022). To mitigate the effects of noise contamination in the measured reflectivity data, the reflectivity values below 15 dBZ were set to zero mm^6/m^3. As an example, Fig. A4 illustrates a radar image in which the 15 dBZ threshold was applied. The result demonstrates that the threshold effectively removes most of the noise while preserving the structure of the storm.

To mitigate the effects of noise contamination in the measured reflectivity data, the reflectivity values below 15 dBZ were set to zero mm^6/m^3 (Doviak and Zrnić, 1993). Additionally, the reflectivity measurements exceeding 53 dBZ were capped at 53 dBZ during the radar rainfall analysis to avoid incorrect interpretations caused by hail (Fulton et al., 1998).

After conducting radar data quality control (Appendix A), data from 2016 to 2022 was compiled and categorized into three datasets. The first dataset comprises 51 storm events, 12 from June to October 2016, 11 from June to August 2017, 6 from September to October 2020, and 22 from May to October 2022, used to evaluate radar composite performance and QI-based bias adjustment. The second dataset comprises continuous data covering August to October 2020 and was used to analyze bias factor uncertainty. The third dataset includes three heavy rainfall events (11th September 2016, 7th June 2017, and 27th September 2020) employed to assess the effectiveness of the QI-based approach in beam-blocked basins. Event selection was based on rain gauge data within the composite area using the Peak Over Threshold (POT) method, with a threshold of 5 mm/h (aligned with the Thai Meteorological Department's (TMD) criterion for moderate rainfall). Events persisted until a rain-free period exceeding two consecutive hours occurred. Events with total rainfall below 25 mm (TMD's heavy rainfall threshold) were excluded. Overlapping events from multiple gauges were consolidated into a single event, and data completeness was verified with radar images. For the analysis of radar composite and bias adjustment, hourly rainfall data were used from 159 tipping-bucket rain gauges; 79 from Hydro-Informatics Institute (HII) with 0.2 mm resolution and 80 from the Department of Water Resources (DWR) with 0.5 mm resolution. To ensure data quality, an initial screening was performed based on measurement integrity. Rain gauges were excluded if more than 80 % of their daily rainfall records fell below the 0.2 mm (HII) or 0.5 mm (DWR) resolution threshold, thereby minimizing the influence of no-rainfall events and potential underreporting. Consistency among gauges was further assessed using double mass curve analysis (Searcy and Hardison, 1960), ensuring agreement between each screened gauge and its neighboring stations. All rain gauges were located within the overlapping area of the Sattahip and Phimai radars (Fig. 1).

4. Methodology

In this section we describe our research set up and the evaluation criteria to assess the performance of our proposed approach. The challenge with radar-based estimates of rainfall is that there is no objective 'true' value. This relates to the fact that, in all cases, radar reflectivity data are empirically bias corrected using ground-based rain gauges. The research consisted of two major steps for the analysis. The first step focused on analyzing the combined quality index (QI) factors for radar compositing. This step introduced an integrated QI framework that incorporates four quality indices, including both static and time-varying components, for use in the composite computation. The second step required conducting a bias adjustment analysis based on the combined QI. An optimal QI threshold was identified to classify bias adjustment factors into high and low quality groups for bias correction. The radar composite estimates were then corrected using QI-based mean field bias adjustment factors (see Eq. (5)) to improve the accuracy of radar-based QPE. The diagram outlining all procedures in this research is shown in Fig. 2.

To evaluate the effectiveness of the combined radar quality indices, both qualitative and quantitative assessments were conducted, as described in section 4.3, to evaluate the performance of the proposed approach. Three independent datasets as detailed in Section 3 were used in this evaluation step. First, 51 storm events were analyzed to assess the radar rainfall composite performance. The leave-one-out procedure was thereafter applied to evaluate the effectiveness of the QI-based bias adjustment based on the same period. Second, continuous three-month dataset were examined to explore the influence of bias factor uncertainty. Finally, the three heavy rainfall events were used to evaluate the QI-based solution in beam-blocked basins.

4.1. Analysis of combined QI factors for radar compositing

To comprehend the impact of various quality indices on composite rainfall assessments in the study area, six combinations of quality indices were introduced for the analysis, as outlined in Table 2. The methods for the analysis are outlined as follows.

1. Convert the measured instantaneous radar reflectivity into an initial radar rainfall intensity using the relationship $Z = 200R^{1.6}$ (Marshall and Palmer, 1948) for individual radars.
2. Compute the radar composite products between the radars by applying the calculated overall QI as the weighted value of the corresponding radar rainfall estimates for each radar station in the overlapping region. For example, in the scenario where all four quality indices were applied, the composite radar rainfall was computed with Eq. (6). For the remaining cases with different combinations of quality indices, the computation was carried out based on the assumptions explained in Table 2.

Table 2
The composite radar rainfall based on six combinations of quality indices.

Distribution code	Overall QI calculation	Methodologies description for radar rainfall compositing
RQI_D	$QI_{i,j} = QI_{D_{i,j}}$	A single QI: associated with the distance from the radar station.
RQI_H	$QI_{i,j} = QI_{H_{i,j}}$	A single QI: associated with the height of the beam above the ground.
RQI_B	$QI_{i,j} = QI_{B_{i,j}}$	A single QI: associated with the beam blockage fraction.
RQI_{DHB}	$QI_{i,j} = QI_{D_{i,j}} \times QI_{H_{i,j}} \times QI_{B_{i,j}}$	Three QIs: combined with the distance from the radar station, the height of the beam above the ground, and the beam blockage fraction.
RQI_F	$QI_{i,j} = QI_{F_{i,j}}$	A single QI: associated with the radar reflectivity fraction.
RQI_{DHBF}	$QI_{i,j} = QI_{D_{i,j}} \times QI_{H_{i,j}} \times QI_{B_{i,j}} \times QI_{F_{i,j}}$	Four QIs: combined with the distance from the radar station, the height of the beam above the ground, the beam blockage fraction, and the radar reflectivity fraction.

$$RQI_{DHBF_j} = \frac{\sum_{i=1}^{N} QI_{i,j} \times R_{i,j}}{\sum_{i=1}^{N} QI_{i,j}} \quad (6)$$

where RQI_{DHBF_j} is the composite radar rainfall (mm) from four QI factors (QI_D, QI_H, QI_B, and QI_F) at pixel j, $R_{i,j}$ for radar station i at pixel j estimated using the relationship $Z = 200R^{1.6}$.

3. Accumulate the composite radar rainfall to obtain a 1-hour radar rainfall products for all cases. The most suitable radar composite product was investigated as described in Section 4.3.1.

4.2. Bias adjustment analysis based on QI specifications

This process begins with determining of the optimal QI threshold, followed by the correction of radar rainfall amounts using a QI-based approach. The following steps outline the process of this exploration.

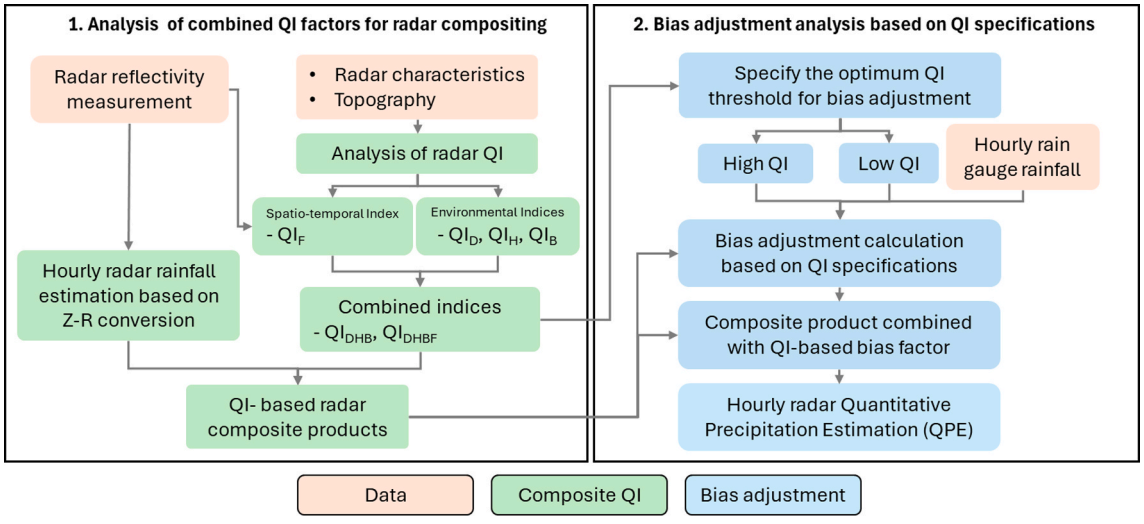

Fig. 2. Diagram of the research methodology workflow, including 1) analysis of combined QI factors for radar compositing, and 2) bias adjustment analysis based on QI specifications.

1. The optimal QI threshold was applied to spatially classify radar-rain gauge pairs within the composite area into high- and low-quality datasets.
2. The MFB analysis, as described in Eq. (5), was performed independently for the high- and low-QI groups, using all radar-rain gauge pairs within each classification to derive group-specific bias adjustment factors.
3. Finally, the estimated MFB factors representing high and low data quality were applied as multipliers to the composited rainfall product at all radar pixels corresponding to each group for hourly radar rainfall correction.

4.3. Evaluation methods for the proposed approaches of radar rainfall products

4.3.1. Investigation of radar rainfall composite performance

In this section, the radar composite performance investigation without bias correction was carried out. The radar composite products obtained from the conventional maximum techniques (R_{MAX}), and those obtained from different individual (RQI_D, RQI_H, RQI_B, and RQI_F) and combined quality index RQI_{DHB}, and RQI_{DHBF} methods, along with rainfall estimates from individual radars, were compared to data from tipping bucket rain gauges located in the composite area using the Root Mean Square Error (RMSE), Normalized RMSE and Mean Bias Error (MBE) as statistical measure. In this analysis, we explored the impact of rainfall intensity and the radar beam blockage on the compositing performance for each technique. The rainfall intensity was categorized into two groups for the analysis: the first encompassing overall rainfall intensity (spanning light to heavy rain intensity) and the second involving only heavy rainfall. According to Thai Meteorological Department (TMD) hourly rainfall criteria, light rain is defined as less than 5 mm/h, moderate rain falls between 5 to 25 mm/h, and heavy rain is considered greater than 25 mm/h. The RMSE and MBE were calculated for each storm event using various composite techniques:

$$RMSE = \sqrt{\frac{\sum_{t=1}^{T}\sum_{c=1}^{N}(G_{c,t} - R_{c,t})^2}{NT}} \tag{7}$$

$$Normalized\ RMSE = \frac{RMSE}{\overline{G}} \tag{8}$$

$$MBE = \frac{1}{NT}\sum_{t=1}^{T}\sum_{c=1}^{N}(G_{c,t} - R_{c,t}) \tag{9}$$

where $G_{c,t}$ = the gauge rainfall (mm/h) at c^{th} gauge for hour t, $R_{c,t}$ = the radar rainfall (mm/h) at gauge c^{th} for hour t, N = total number of rain gauges in the analysis. T is the total number of time periods for each storm event used in the calculation, with a timestep interval of 1 h. $\overline{G}$ is the mean hourly gauge rainfall for the corresponding dataset (mm/h).

To qualitatively evaluate the performance of the radar composite, an effective composite method should retain high-quality data while minimizing the impact of poor measurements and inconsistencies from multiple radar stations, ensuring a smooth and coherent representation of storm structures. The effectiveness of this approach is assessed using the smoothness index as suggested by Ośródka et al. (2014) and Ośródka and Szturc (2015),

$$ENL_i = \frac{\mu^2(X)}{var(X)} = \frac{\left(\frac{1}{m}\sum_{i=1}^{m}x_j\right)^2}{\frac{1}{m}\sum_{i=1}^{m}\left(x_j - \frac{1}{m}\sum_{i=1}^{m}x_j\right)^2} \tag{10}$$

$$smoothness = \frac{\sum_{i=0}^{n-1}ENL_i}{\sum_{i=0}^{n-1}x_i} \tag{11}$$

where j is the number of radar pixel within the vicinity of the i-pixel, with j ∈ (1, …, m), In this study, the 11 km × 11 km grids were used (i.e., $m = 121$).

In this study, the smoothness index was computed on an event basis to reduce the influence of temporal variability in rainfall intensity and to characterize storm behavior across the composite area and its surrounding regions. The analysis of smoothness was calculated within and around the composite area, to assess the spatial variability of the radar rainfall product and evaluate the qualitative performance of composite methods. A higher smoothness reflects that the radar rainfall product provides a more spatially uniform rainfall pattern across the region. Additionally, greater smoothness suggests that merging of data from multiple radar stations effectively reduces inconsistencies, resulting in a more reliable and continuous representation of rainfall patterns, particularly along the edges of the composite area.

4.3.2. Determination of the optimal QI threshold for bias adjustment

The optimal QI threshold is crucial for spatially classifying radar–rain gauge pairs within the composite area into high- and low-quality datasets, which can significantly impact the accuracy of the bias adjustment. The following steps outline the procedure used in this investigation.

1. The results obtained from calculating the overall QI and the radar composite products as mentioned in Eqs. (2) and (4), respectively, were used as initial data in this analysis.
2. Identify various QI threshold values ranging from 0.7 to 0.9 with an interval step of 0.05 (five cases of simulation) to separate 159 rain gauges located in the composite area into high and low-quality datasets for every rainfall event.
3. Calculate the QI-based MFB associated with the five cases of QI thresholds using the methodology proposed in Eq. (5). For each bias adjustment calculation case, one rain gauge (from 159) was systematically left out for evaluation, and the remaining rain gauges were used to calculate the bias adjustment factor for all five different QI thresholds. This leave-one-out cross-validation process was applied iteratively across all available gauges and repeated for each hourly time step. The procedure was conducted for all hourly time steps and all combinations.
4. The error of radar rainfall estimates after correcting with the estimated bias factor at each radar pixel corresponding to the discarded gauge was evaluated for all trials. Root Mean Square Error (RMSE) was applied as the objective function to determine the optimal QI threshold.

4.3.3. Assessing the influence of radar data quality on uncertainties in bias adjustment factors

A bias factor of 1.0 indicates perfect agreement between radar estimates and rain gauge measurements. However, bias factors greater than 5 or less than 0.2 are generally considered outliers and are excluded from calculations to minimize uncertainty and ensure more reliable results (Chumchean et al., 2006). For meaningful rain radar estimates of rainfall, the bias adjustment factor should not behave too spurious over time. We analyzed the variation in hourly MFB across radar rainfall data of differing quality from August to October 2020. To mitigate fluctuations in the bias factor's variability, logarithmic transformations of bias factors were applied. Three radar rainfall datasets with different data quality levels were tested to evaluate their influence on MFB uncertainties: individual radar data from Sattahip and Phimai (pre-compositing), and the composite product RQI_{DHBF}. To assess the uncertainty of bias adjustment factors, we compared the probability density function of the logarithmic MFB from August to October 2020 across different radar rainfall products, rainfall intensities, and radar quality levels. The analysis considered both the standard deviation and the probability of bias factors falling within the recommended range of 0.2 to 5, corresponding to a factor 5 underestimation to a factor 5 overestimation to quantify uncertainty.

4.3.4. Evaluating the effectiveness of QI-based bias adjustment for heavy rainfall estimates

The study focused on assessing the accuracy of the estimated QI-based composite radar rainfall with the bias adjustment (RQI_{DHBF}-MFB_{QI}) for heavy rainfall, particularly in areas with low data quality due to beam blockage. We compared our methodology with the conventional MAX and MFB technique (R_{MAX}-MFB). The evaluation involved radar rainfall estimates before and after applying the bias correction techniques, categorized into four cases based on rainfall intensity and the locations of the rain gauges (Table 3). For each evaluation case, the number of rain gauges in the specified areas (with one gauge left out for validation) was used to compute the corresponding bias adjustment factors. Hourly RMSE and MBE were determined for different radar rainfall products at the left-out rain gauge for each storm event.

Three severe rainfall events occurring in four beam blockage areas during September 2016, June 2017, September 2020 were selected for this investigation. Initially, both the RQI_{DHBF}-MFB_{QI} and the R_{MAX}-MFB methods were used to compare the accuracy of radar rainfall estimates with available rain gauge data for each storm. Subsequently, spatial rainfall estimates were generated for the four beam-blocked basins: the Lower Pasak, Chao Phraya, Nakhon Nayok, and Upper Bang Pakong.

5. Results and discussions

5.1. Spatial and temporal variations of the radar quality indices

Among the six combinations of QI factors used for radar compositing in this study (Table 2), four quality indices (QI_D, QI_H, QI_B, and QI_{DHB}) were classified as spatially varying, reflecting environmental factors specific to each radar. These indices are spatially variable but remain constant over time (Fig. 3a), as they are derived from radar beam characteristics and topographic features. Logically, the QI_D values for both Sattahip and Phimai range from 1 at the radar site to 0 at the maximum radar radius of 240 km. Since this study used 2.5 km CAPPI data for both Sattahip (at 139 km) and Phimai (at 136 km), the QI_H values range from 1 at the radar station to 0.7 at 136/139 km distance from the radar, with some exceptions between 136/139 and 240 km distance due to the lowest PPI (0.5°) scans and mountain elevation. Furthermore, the QI_B factor provides clear identification of blockage areas and their severity for each radar station. This capability extends to identifying minor blockage areas that may not be readily visible in the radar image. The combination of distance, height and beam blockages (QI_{DHB}) gives lower final QI values (Fig. 3a, lowest panel).

To include the temporal variation in radar reflectivity signal, we added the reflectivity index QI_F (Fig. 3). Here we show two QIs, namely QI_F, and QI_{DHBF}, which exhibit spatiotemporal variation per timestep in the overlapping areas. The variability of the QI_F is influenced by radar system characteristics and changing storm patterns in both space and time. A noticeable contrast in QI_F between the Sattahip and Phimai radar stations is particularly evident in areas affected by beam blockage, where the measurements from one radar are underestimated. Meanwhile, QI_{DHBF} accounts for four factors influencing radar measurement quality. When applying this combined QI, its value is reduced to reflect the influence of various factors in the QI scheme, particularly in beam blockage areas. Radar composite products for the six QI combinations were subsequently generated by applying the calculated overall QI as a weighting factor to the corresponding radar rainfall estimates from each radar station within the overlapping region.

Table 3
Cases for evaluating the effectiveness of bias correction techniques.

Cases	Rainfall classification	Rainfall intensity (mm/h)	Boundary specification	Number of rain gauges for evaluation
1	Overall rainfall intensity	> 0.1	In the composite area	159
2	Heavy rainfall	> 25	In the composite area	159
3	Overall rainfall intensity	> 0.1	In the region with low-quality radar data	23
4	Heavy rainfall	> 25	In the region with low-quality radar data	23

5.2. Qualitative performance of radar composite methods

Without compositing, the Sattahip radar produced higher rainfall amounts than the Phimai radar within the composite area (Fig. 4), highlighting the impact of beam blockage in the Phimai coverage area. After compositing, R_{MAX} produced a product similar to Sattahip, because it mainly used data from this radar as the maximum values. This reliance can lead to a noticeable discontinuity in the storm cell at the edge of radar composite area, particularly when the maximum value is chosen from Sattahip. In contrast, all QI products could smooth out the transition along the edge and provide a more continuous rainfall pattern. They display lower rainfall amounts compared to those obtained from R_{MAX}, as they incorporate values from the Phimai radar, which generally estimates less rainfall than Sattahip. Additionally, RQI_D and RQI_H may not adequately compensate for missing radar data in beam blockage areas, whereas RQI_B and RQI_F could address this issue more effectively. The RQI_F appears to generate a smoother storm pattern than RQI_B because, while RQI_B assigns equal weight to each radar in the areas unaffected by beam blockage, RQI_F considers measurement differences and preserves the storm pattern. The combined index QI_{DHB} typically provides lower rainfall estimates than QI_{DHBF}, as it considers only static environmental factors without adjusting for the systematically lower reflectivity values from the Phimai radar compared to the Sattahip radar. In contrast, QI_{DHBF} incorporates both environmental and observational factors, effectively mitigating measurement inconsistencies and resulting in higher rainfall totals and a more spatially continuous and realistic storm structure.

The average smoothness index across the total of 51 storm events among the compositing techniques as shown in Fig. 5 indicates that the smoothness indices for all the Quality Index methods are obviously higher than that of the R_{MAX} method for most events. The RQI_{DHBF} shows the greatest smoothness, indicating that it generates the rainfall field with the lowest spatial variability in the composite area, particularly in the beam-blocked regions and along the composite edges. This improvement in smoothness ranges from 2 % to 20 % compared to the R_{MAX} method. These results suggest that the RQI_{DHBF} method produces a smoother and more consistent representation of storm structures, outperforming the other methods, particularly the traditional R_{MAX} approach. Examples of radar composite products generated using the R_{MAX} and RQI_{DHBF} methods for four storm events are presented in Fig. B1 in Appendix B for reference.

5.3. Quantitative evaluation of radar composite methods at rain gauge locations

Fig. 6 shows the accuracy of each composite method across various rainfall intensities in the 51 events. As Sattahip typically gives higher reflectivity values than Phimai, the radar rainfall estimates based exclusively on Phimai data tend to underestimate rainfall, especially during heavy events. This results in the highest mean RMSE for Phimai across all cases. However, after compositing, the accuracy of radar rainfall estimates improves across all rainfall intensity criteria. The variation of the RMSE for RQI_D, RQI_H, and RQI_B show similar distributions, particularly when using all rainfall events. In the heavy rainfall cases, the RQI_F improves the RMSE by 6.2 % for the mean and 5.5 % for the lower 25th percentile, compared to the RQI_B. Applying RQI_{DHBF} results in the best performance of radar composite products across all storm types. The RQI_{DHBF} can improve the median RMSE by 6.5 %, 20.8

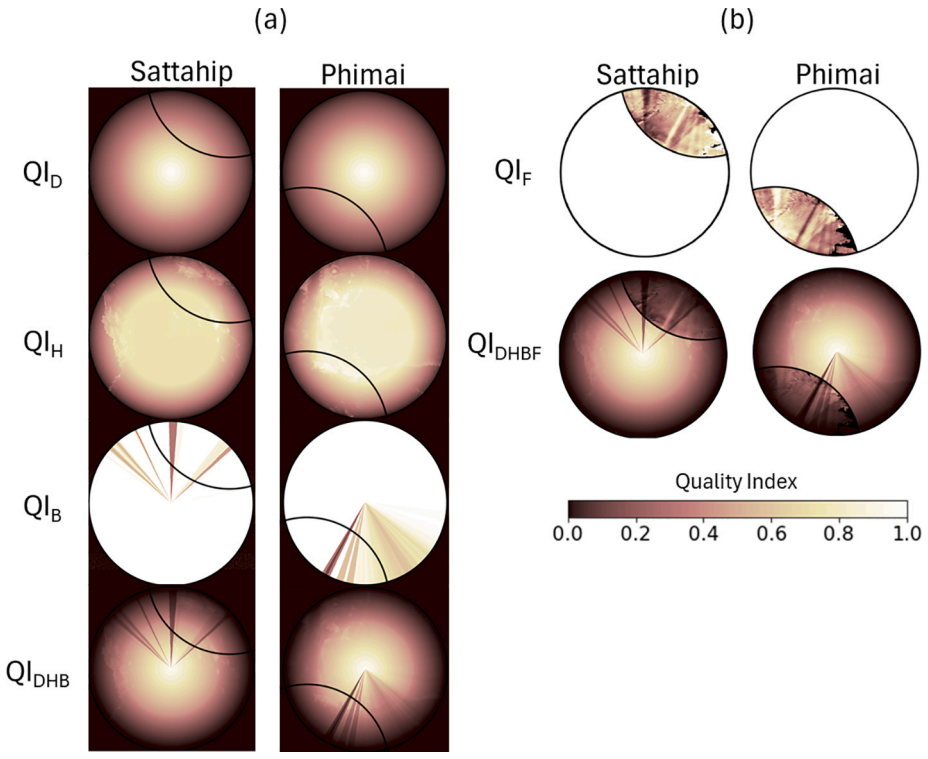

Fig. 3. Variation of various radar Quality Index (QI) factors for different combinations of the Sattahip and Phimai radars: (a) spatial variation of QI_D, QI_H, QI_B and QI_{DHB}, (b) spatiotemporal variation of QI_F, and QI_{DHBF}.

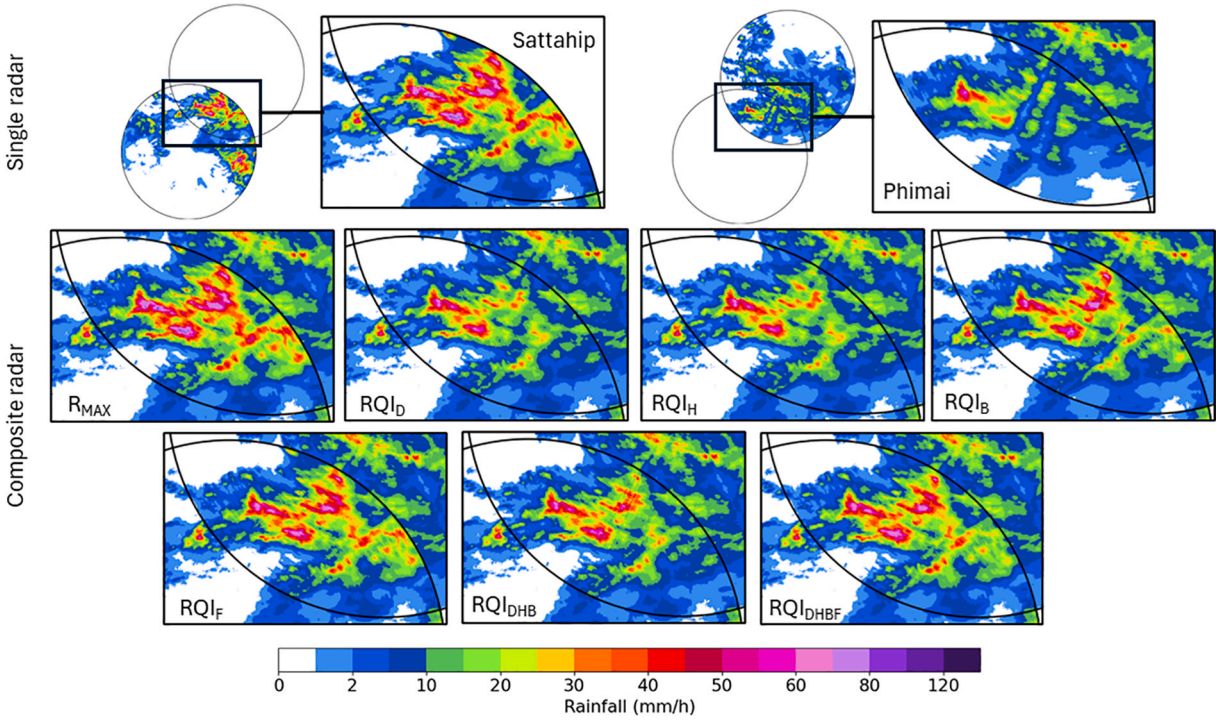

Fig. 4. Example of spatial accumulated rainfall patterns using various techniques during the event on May 16, 2022, from 15:00 to 21:00 LST.

%, and 5.6 % compared to the Sattahip, Phimai, and R_{MAX}, respectively, in heavy rainfall. Furthermore, an analysis of the mean RMSE values relative to the corresponding mean hourly gauge rainfall (normalized RMSE) across the panels in Fig. 6 reveals that the normalized RMSE for RQI_{DHBF} is highest for light to moderate rainfall events (81 %) but lowest for heavy rainfall events (59 %).

To evaluate the spatial accuracy of each composite method, the RMSE at rain gauge locations within the composite area was computed (Fig. 7). In beam blocked regions, Sattahip underperformed compared to the Phimai. However, R_{MAX} effectively compensated for errors between the two radars. The RQI_F emerged as the most effective single quality index in both affected and unaffected areas, while RQ_B appeared to be

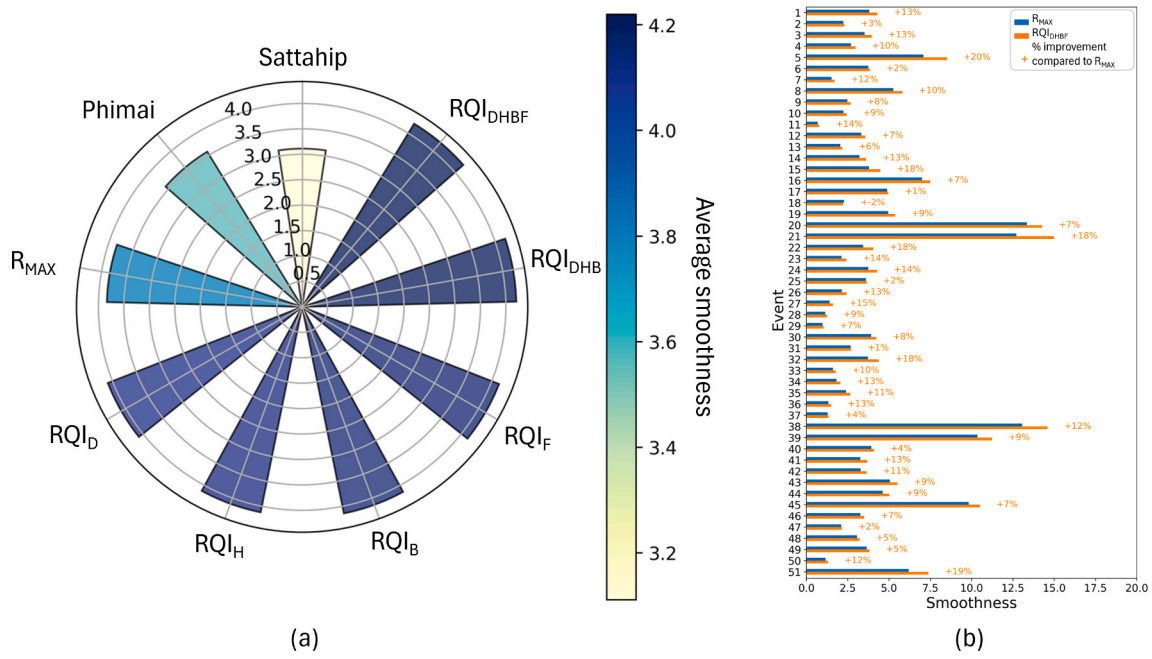

Fig. 5. Qualitative evaluation of the radar composite method using smoothness index. (a) Average smoothness across 51 rainfall events for each radar method, and (b) Event-based smoothness comparison between R_{MAX} and RQI_{DHBF}, along with the percentage improvement of RQI_{DHBF} compared to R_{MAX}.

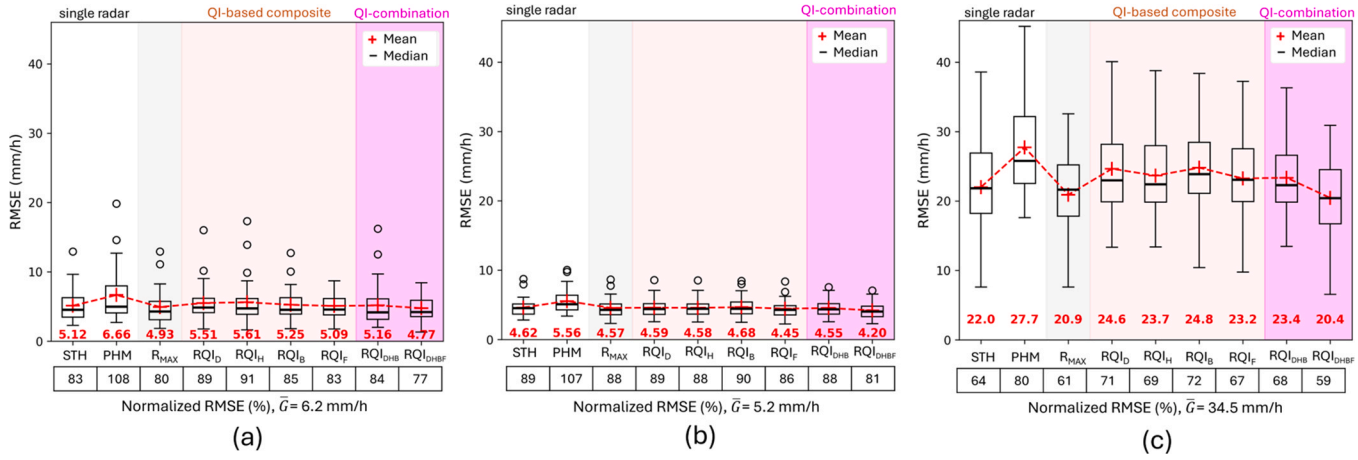

Fig. 6. Comparison of the event based RMSE for different radar products for (a) overall rainfall events (b) light to moderate rainfall events, and (c) heavy rainfall events.

practical only in the contaminated area. Among combined indices, RQI_{DHBF} achieved the lowest median of RMSE in both types of areas, improving the median RMSE by 36.5 % and 20.4 % compared to the Sattahip and Phimai in beam-blocked areas. Additionally, the normalized RMSE for RQI_{DHBF} was found to be higher in beam-blocked areas (72 %) compared to unaffected areas (51 %), showing a difference of approximately 21 %.

5.4. *Influence of QI threshold on the bias adjustment solution*

The average spatio-temporal variation of the QI_{DHBF} across 51 events in the overlapping area is shown in Fig. 8. The distribution of overall QI_{DHBF} values ranges from 0.42 to 0.93 (Fig. 8b). The values at the 75th and 25th percentiles fall within the range of 0.69 to 0.86.

We also assessed the impact of the QI threshold on the bias adjustment results (Fig. 9). Hereto, the hourly MFB_{QI} values were calculated for radar rainfall correction across each threshold, with RMSE used to evaluate performance related to rain gauge data. The RMSE remains low when there are more high-quality data pairs than low-quality ones (Fig. 9a), but rises sharply when the low-quality data pairs become predominant. A QI threshold value of 0.80, separating 85 % of data pairs into high-quality and 15 % into low-quality, led to the minimum RMSE of 4.46 mm/h with a normalized RMSE of approximately 72 %.

A lower number of data pairs for each data group reflects higher median values and spread in the MFB factors (Fig. 9b). The optimal QI threshold of 0.80 minimizes the spread of the MFB factors for high-quality and reduces uncertainty in the low-quality dataset. In addition, this threshold effectively distinguishes bias values between good and poor-quality radar pixels. For the high- and low-quality datasets, the MFB values at the 25th and 75th percentiles range from 1.06 to 1.86 and from 1.02 to 2.16, respectively, with median MFB values of 1.40 and 1.55.

Not surprisingly, most low-quality data is located in the beam blockage areas, where radar rainfall is typically underestimated (Fig. 9c, using QI threshold of 0.8). Therefore, rain gauge locations with QI values below 0.8 understandably require higher bias adjustment factors

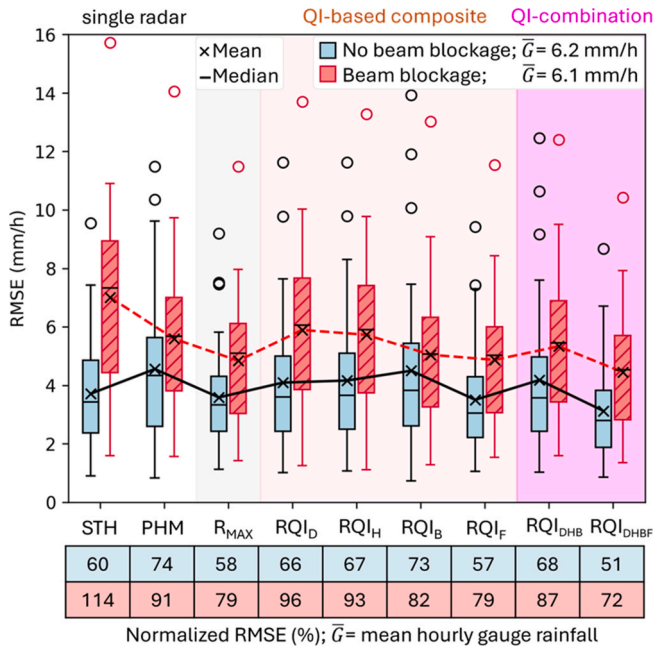

Fig. 7. Variation in event based RMSE for the various quality index methods at the rain gauges located in the area unaffected by beam blockage and that affected by beam blockage.

than areas with QI values above this threshold (Fig. 9b). These results emphasize the effectiveness of the developed QI_{DHBF} and optimal QI threshold in detecting data quality and their corresponding bias adjustment factors. This optimum threshold was employed for evaluating the effectiveness of the bias adjustment analysis using the MFB_{QI} technique.

5.5. *Influence of radar data quality on the bias adjustment factor uncertainties*

The variation of the hourly bias factors corresponding to radar rainfall with three datasets from August to October 2020 is shown in Fig. 10. The dashed lines in the figure represent the recommended bias limits range from 0.2 to 5 (i.e. a factor 5 underestimation (a factor ⅕) to a factor 5 overestimation). The results show significant uncertainty in the hourly logarithmic MFB across all products, related to the high variability in the average rain gauge rainfall used for MFB calculations. While most MFB values remain within the bias limits, some outliers are evident. The radar products from the individual radars, Sattahip and particularly Phimai, show greater uncertainty in bias estimates, with Phimai exhibiting the highest standard deviation. On the other hand, the composite product RQI_{DHBF} demonstrates the least outliers and the lowest standard deviation in the bias factor time series, indicating better stability compared to the individual radars.

The probability density functions of the logarithmic MFB (Fig. 11) show significant variability depending on radar data quality and rainfall intensities. The Phimai product exhibits notably higher variability in bias factors than Sattahip, likely due to its lower radar measurement quality. However, the RQI_{DHBF} effectively reduces bias factor uncertainties, resulting in the lowest standard deviation, especially during heavy rainfall events above the 90th percentile. A similar pattern is observed when calculating MFB using only high-quality radar-rain gauge pairs ($MFB_{QI\text{-}high}$), as the number of high-quality data pairs aligns closely with those from all stations.

On the other hand, selecting radar-rain gauge pairs from low-quality radar data locations ($MFB_{QI\text{-}low}$) shows similar bias patterns across individual radar products, with the greatest bias uncertainty found in these poor-quality regions. Notably, the RQI_{DHBF} product explicitly reduces variability, achieving the lowest standard deviation compared to both Sattahip and Phimai, with strong performance improvement observed during heavy rainfall events (90th percentile). In this case, the probability that the bias factors fall within the range of a factor ⅕ to a factor 5 (P(⅕,5)) for the RQI_{DHBF} reaches 0.93, compared to 0.76 for Sattahip and 0.83 for Phimai. This demonstrates that the composite technique substantially enhances reliability and reduces uncertainties in bias adjustment, particularly in low quality dataset with high-intensity rain scenarios.

5.6. *Effectiveness evaluation of QI-based bias adjustment for heavy rainfall at rain gauge locations*

The results of four cases (see Table 3) show that combining the MFB with R_{MAX} and MFB_{QI} with RQI_{DHBF} enhances the accuracy of radar rainfall estimates, especially for the heavy rainfall scenarios (Fig. 12). Additionally, it is evident that the RQI_{DHBF}-MFB_{QI} improves radar rainfall estimates more effectively than the R_{MAX}-MFB for all simulations. The rainfall estimates in the composite area (Figs. 12a) and 13b) are significantly improved when using RQI_{DHBF}-MFB_{QI} for heavy rainfall

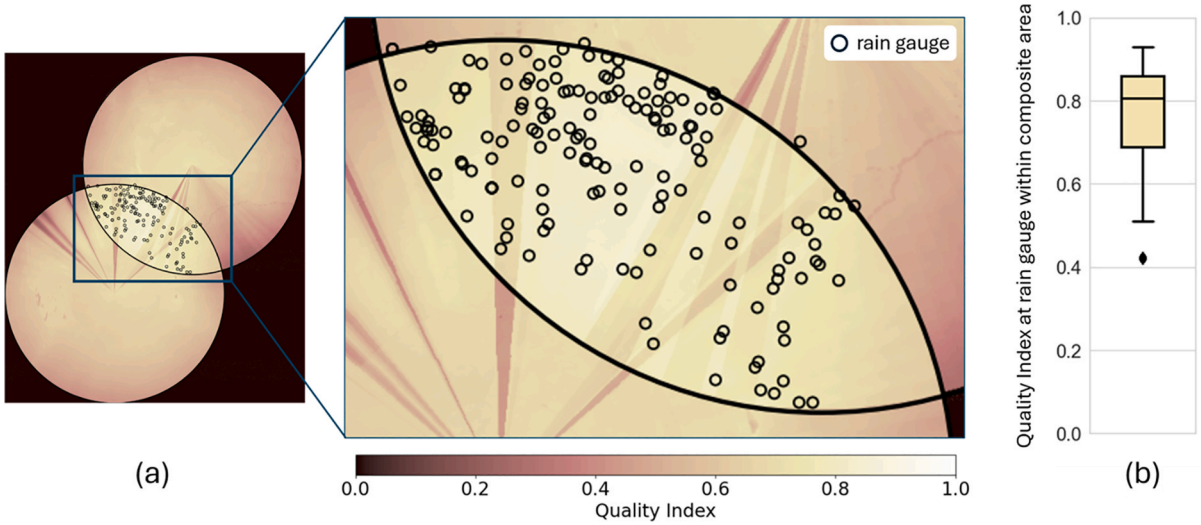

Fig. 8. Distribution of the overall QI_{DHBF} in the composite area. Panel a) shows the average spatio-temporal distribution of QI_{DHBF} across all events in the overlapping area, and panel (b) shows distribution of QI_{DHBF} values at all rain gauges for 51 storm events.

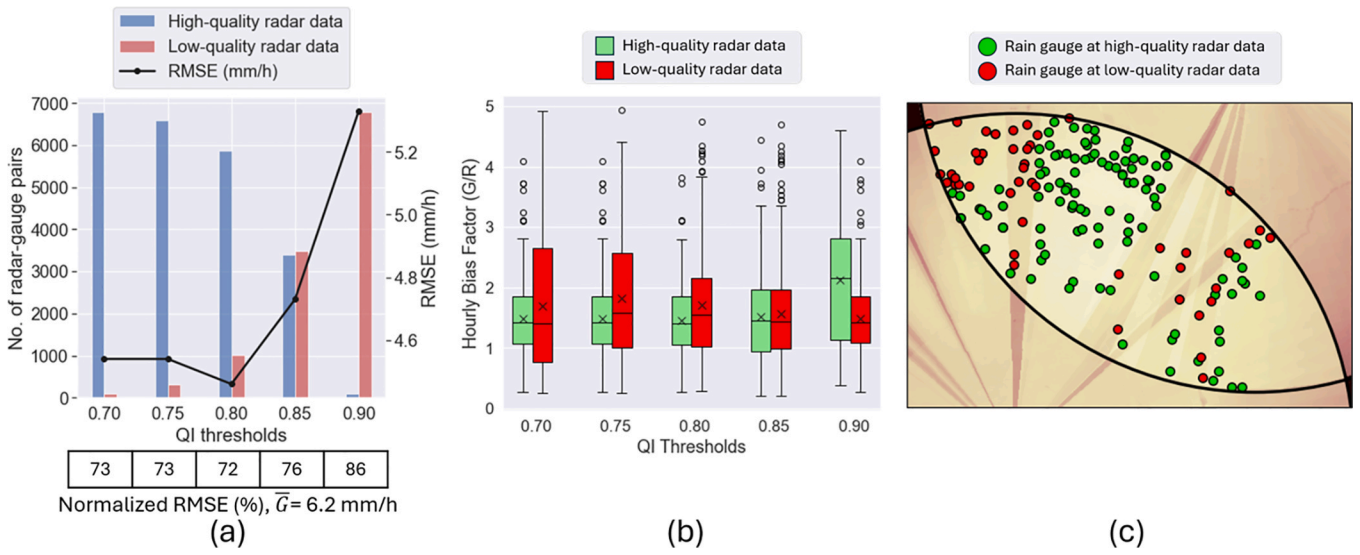

Fig. 9. Comparison of (a) the number of data pairs with high and low-quality datasets for the bias adjustments and corresponding RMSE for each QI threshold and (b) the hourly bias adjustment factor for different quality datasets of the corresponding QI thresholds, (c) spatial classification of radar pixels at corresponding rain gauge locations having average QI (over 51 storm events) above and below the threshold of 0.8.

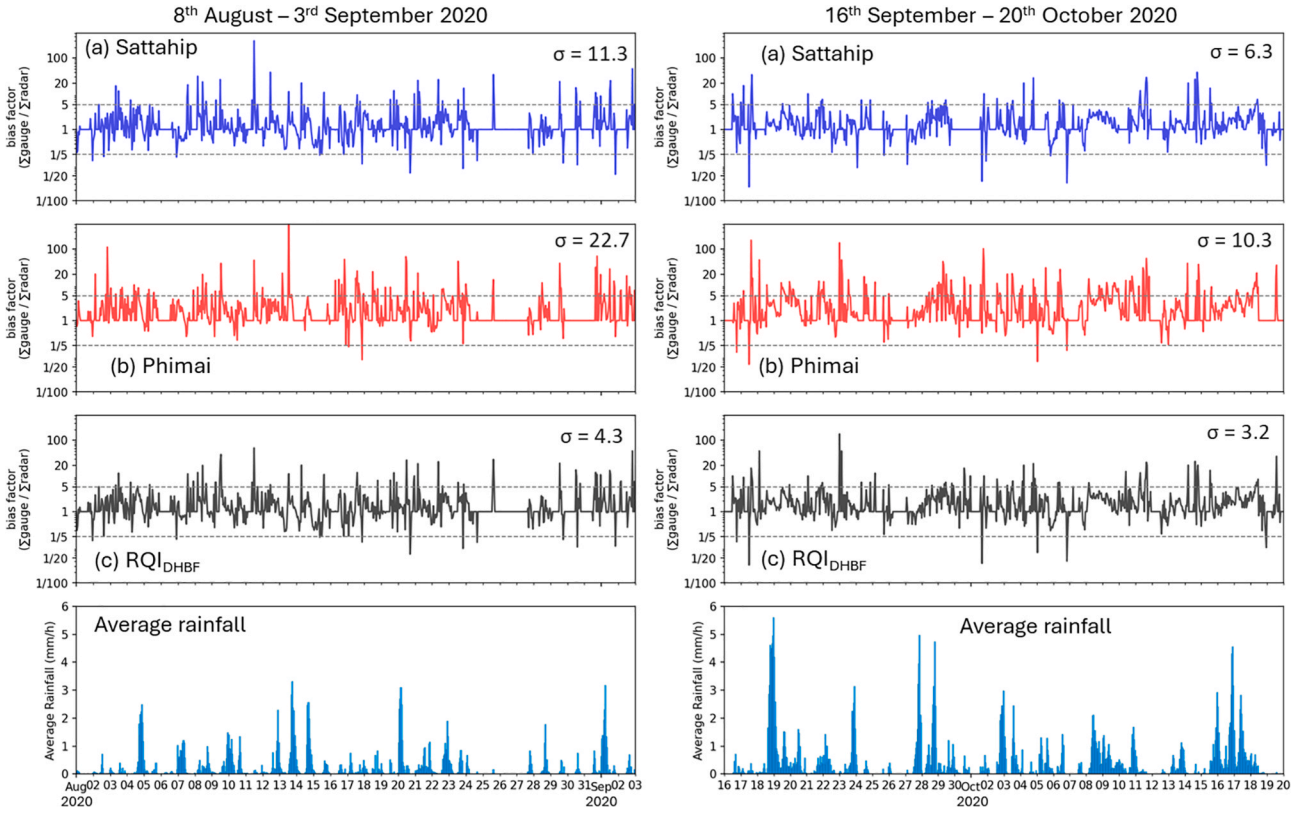

Fig. 10. Time series plot of logarithmic hourly bias factors from August to October 2020 for different radar quality products: (a) Sattahip radar (b) Phimai radar and (c) the composite product RQI$_{DHBF}$.

scenarios. The mean RMSE (the black line in Fig. 12) is reduced from approximately 16.3 to 13.9 mm/h for Case 2. The mean MBE changes from approximately 14.7 to 13.0 mm/h (red dotted line Fig. 12). The latter indicates a reduction in the underestimation of radar rainfall when using the RQI$_{DHBF}$-MFB$_{QI}$. Interestingly, there is a marginal reduction in mean RMSE and MBE improvement across overall rainfall intensity for Case 1. In this case, the mean RMSE is marginally lowered from 4.5 to 4.4 mm/h, and the mean MBE changes from 0.3 to 0.1 mm/h. In regions with low-quality radar data, a much clearer improvement is observed during heavy rainfall events (Case 4) in the mean RMSE values with the RQI$_{DHBF}$-MFB$_{QI}$ method, compared to the entire composite region (Case 2) (Fig. 12b-c). The mean RMSE decreases from about 16.7 to 12.8 mm/h, and the mean MBE shifts from 16.6 to 13.2 mm/h when comparing R$_{MAX}$-MFB to RQI$_{DHBF}$-MFB$_{QI}$. This demonstrates a notable reduction in underestimation errors and improves accuracy in radar rainfall estimation for heavy rainfall using the RQI$_{DHBF}$-MFB$_{QI}$ method. Analysis of the

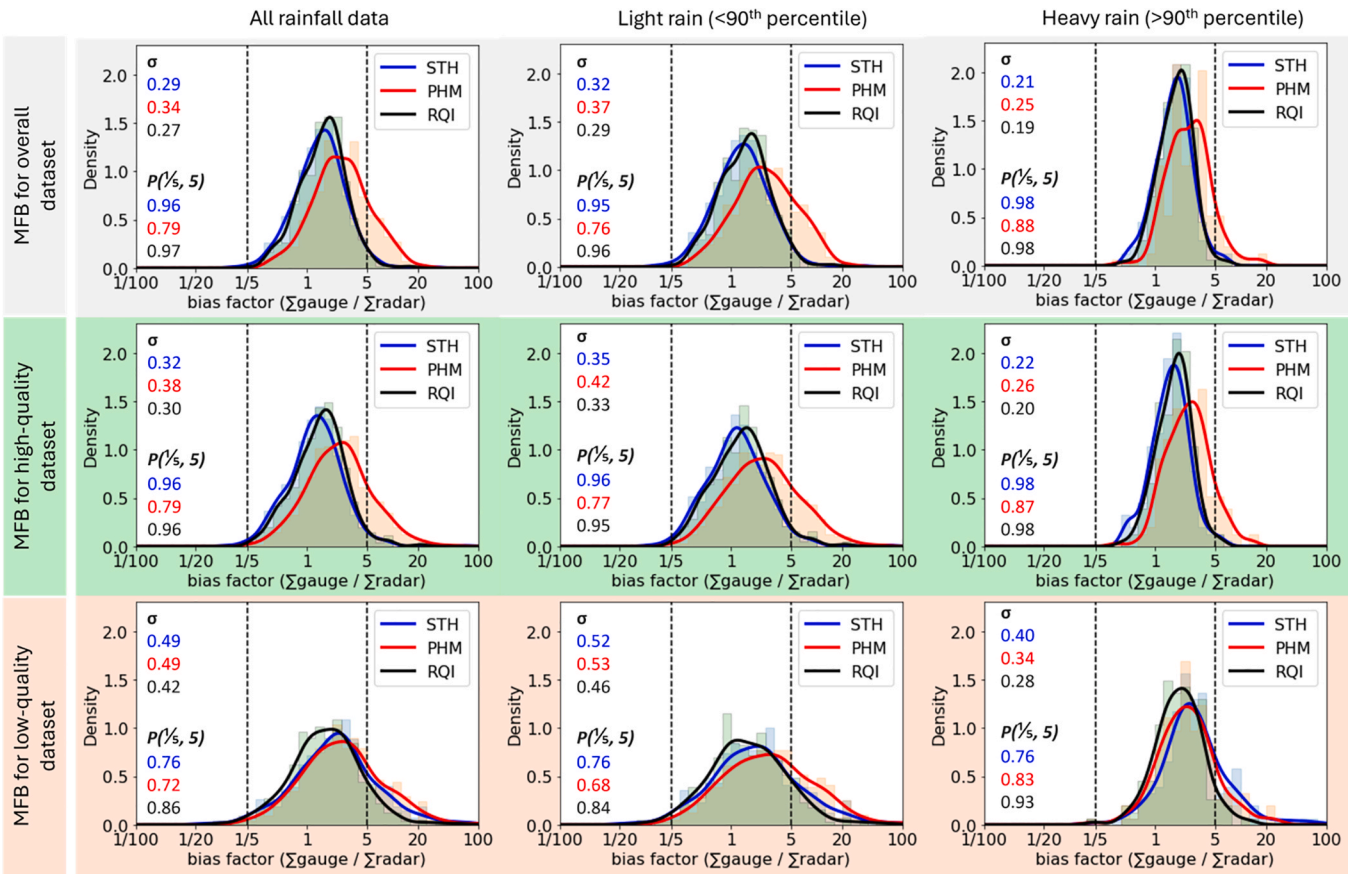

Fig. 11. Probability density function of logarithmic bias factors for different radar rainfall products, rainfall intensities, and radar quality levels.

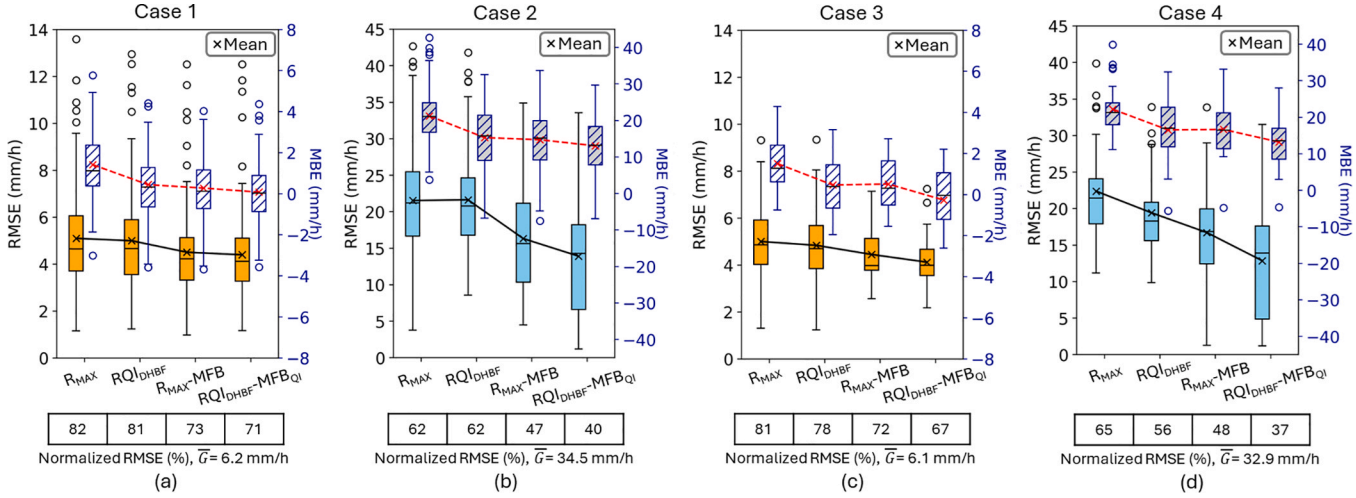

Fig. 12. Comparison of the RMSE among various techniques for different cases of: (a) overall rainfall intensity in the composite area, (b) heavy rainfall in the composite area, (c) overall rainfall intensity in the region with low-quality radar data, (d) heavy rainfall in the region with low-quality radar data.

normalized RMSE across four panels in Fig. 12 shows that the mean RMSE is significantly lower for heavy rainfall events compared to overall cases. Specifically, the normalized RMSE for RQI_{DHBF}-MFB_{QI} in heavy rainfall cases is approximately 30 % lower than for all intensity cases.

It is noted that the boxplot reveals a broader distribution of between the 25th and 75th percentile for heavy rainfall scenarios (Case 2 and Case 4) compared to the overall rainfall intensity, both in the entire composite and in the low-quality locations. This higher variation could be related to the lower number of radar-rain gauge pairs during the heavy rainfall events, leading to increased spatial uncertainty in the mean field bias adjustment factor. For further evaluation, the influence of rain gauge network density on the uncertainty of radar rainfall estimates can be found in Appendix C.

5.7. Estimation of spatial heavy rainfall over the beam blocked basins

Fig. 13(b–d) illustrates that the R_{MAX}-MFB method failed to capture the rainfall storm in the signal-blocked areas (Fig. 13 (a) reflecting a key

limitation of the conventional maximum approach. In contrast, the RQI_B-MFB_{QI} method, which incorporates beam blockage information through the QI_B index, more effectively detects rainfall in obstructed regions. However, outside of beam-blocked zones, the RQI_B-MFB_{QI} method tends to underestimate rainfall, likely due to its equal weighting of all radar inputs, without accounting for the distance from radar, beam height, or reflectivity differences. The RQI_{DHBF}-MFB_{QI} method, which integrates four quality indices, QI_D, QI_H, QI_B, and QI_F, effectively delineated heavy rainfall across both obstructed and unobstructed regions. Moreover, the hourly rainfall distribution patterns of the RQI_{DHBF}-MFB_{QI} appear to be more similar to the rain gauge data than those of the RQI_B-MFB_{QI} and R_{MAX}-MFB, respectively across all tested events (Fig. 13b–d).

The RQI_{DHBF}–MFB_{QI} method significantly improved the RMSE for the three events, with values ranging from 1.8 to 7.1 mm, compared to 3.7 to 8.7 mm for RQI_B-MFB_{QI} and 4.1 to 13.7 mm for R_{MAX}-MFB. The greatest improvement, 56.2 % reduction in RMSE relative to R_{MAX}-MFB was observed for the event on June 7, 2017, from 19:00 to 20:00 LST. Fig. 13 shows that the R_{MAX}-MFB consistently gave positive MBE values (2.0–2.7 mm/h), indicating an underestimation in the blocked areas across all cases. Incorporating beam blockage information in RQI_B-MFB_{QI} reduced MBE to −1.7 to 1.9 mm/h, while the RQI_{DHBF}–MFB_{QI} produced slightly overestimated results, with MBE values ranging from −1.7 to 0.5 mm/h. Overall, these results demonstrate that the integrated multi-index approach of RQI_{DHBF}–MFB_{QI} delivers the most accurate rainfall estimates, outperforming both single-index and conventional compositing methods.

Additionally, an estimation of spatial rainfall over the four beam-blocked basins was conducted by comparing the performance of RQI_{DHBF}–MFB_{QI} and R_{MAX}-MFB products (Fig. 14). It is evident that the RQI_{DHBF}–MFB_{QI} gave basin-average rainfall amounts 21.7 % to 55.8 % higher than R_{MAX}-MFB. This suggests that the conventional R_{MAX}-MFB method, which used all available radar-rain gauge pairs without accounting for the quality of radar observations, can significantly underestimate heavy rainfall in the signal-blocked regions. In contrast, the RQI_{DHBF}–MFB_{QI} approach demonstrates the ability to categorize bias correction factors based on each data quality category, leading to a substantially improvement in heavy rainfall estimates in these obstructed areas.

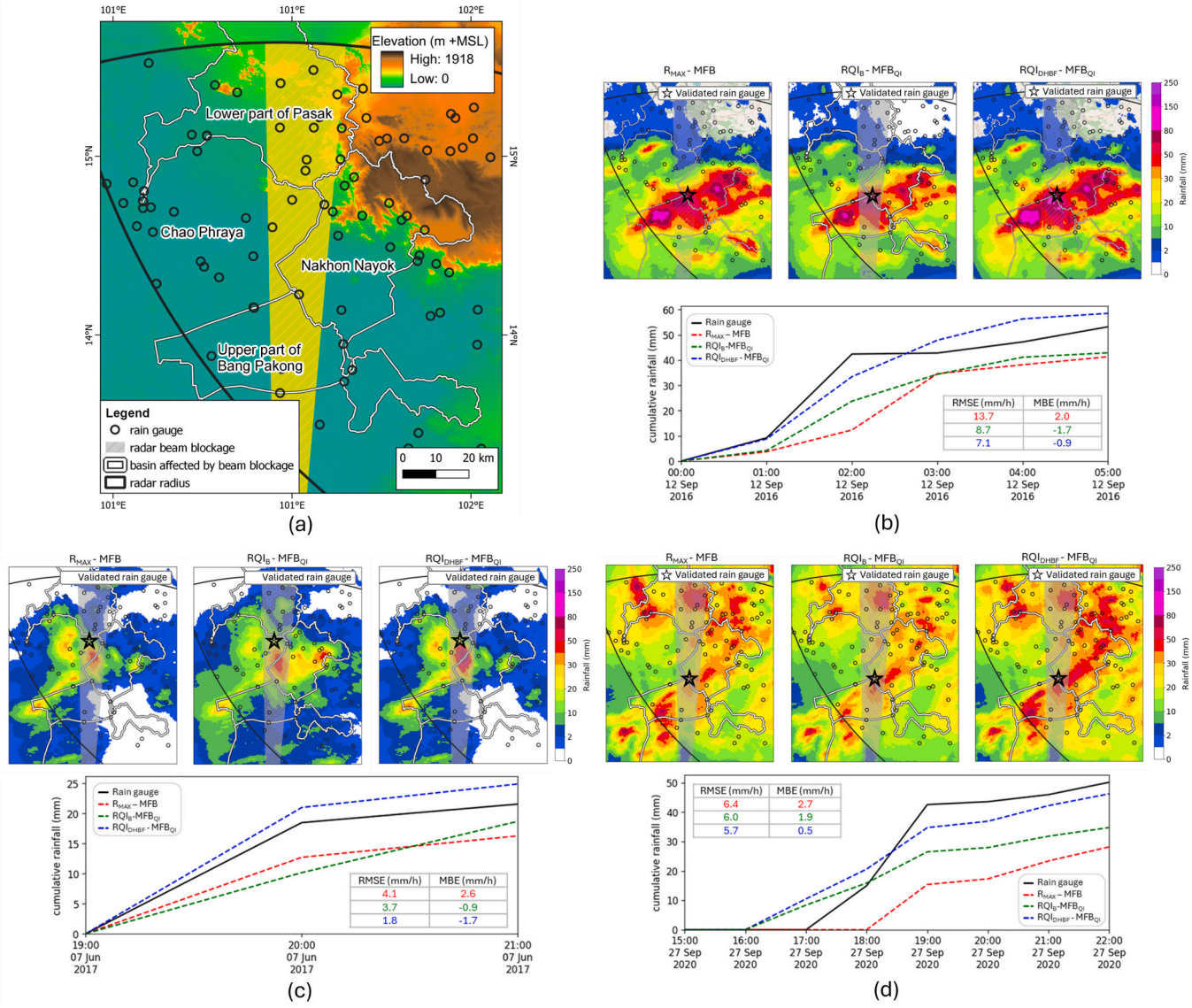

Fig. 13. The analysis of spatial radar rainfall over basins affected by beam blockage. Panel (a) displays the four basins within the composite area affected by beam blockage. Comparison of spatial radar composite with R_{MAX} – MFB, RQI_B – MFB_{QI}, and RQI_{DHBF} – MFB_{QI} and corresponding mass curves for rainfall events: (b) from September 11, 2016, at 23:00 to September 12, 2016 at 07:00 LST, (c) from June 07, 2017 at 19:00 to 20:00 LST, (d) from September 27, 2020 at 15:00 to 22:00 LST.

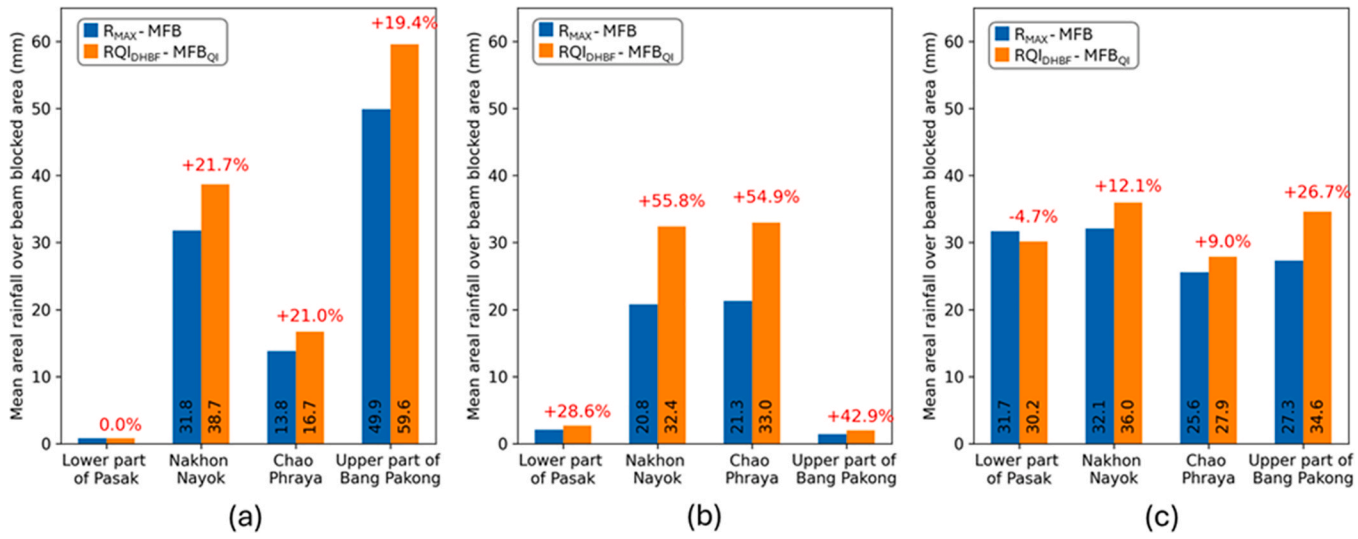

Fig. 14. Comparison of areal average rainfall over basins affected by beam blockage in mm and percentage of difference between radar composite with R_{MAX} – MFB and RQI_{DHBF} – MFB_{QI} for rainfall events: (a) from September 11, 2016, at 23:00 to September 12, 2016, at 07:00 LST, (b) from June 07, 2017, at 19:00 to 20:00 LST, (c) from September 27, 2020 at 15:00 to 22:00 LST.

6. Conclusion

This study introduced an advancement in composite radar rainfall estimation techniques, focusing specifically on heavy rainfall events in mountainous regions. We proposed a novel spatio-temporal Quality Index scheme designed to address the variability in reflectivity data from individual radars caused by diverse hardware and environmental properties. Our approach captured the spatial and temporal variations in radar measurements between overlapping radar domains and effectively identifies beam blockage areas, enhancing radar composite performance over conventional methods like the maximum method. The method effectively addressed the issue of displaying discontinuities in storm cells, thereby improving the coherence and accuracy of radar imagery. Notably, the proposed radar reflectivity fraction proved to be the most effective single quality index for mitigating differences in reflectivity measurements caused by radar miscalibration. Nevertheless, we strongly recommend that weather radars to be properly calibrated as a critical step toward improving the accuracy of radar observations and the reliability of subsequent analyses.

Furthermore, the study developed a novel bias adjustment technique by integrating the combined spatio-temporal Quality Index to distinguish the bias adjustment factors associated with radar data quality categories. In our case study, it was determined that a QI threshold value of 0.80, which separates 85 % and 15 % of the entire data pair into high- and low-quality data groups, was optimal. This threshold effectively minimizes MFB factor variability, reduces uncertainty in low-quality data. Notably, it was evident that the locations of the poor-quality dataset mostly coincide with the beam blockage areas, resulting in lower bias factors for these regions compared with the high-quality dataset. Assessing the influence of radar data quality on the bias factor uncertainties revealed that significant uncertainties influenced by both radar data quality and rainfall intensities. The composite product effectively mitigated uncertainties, particularly during heavy rainfall events, and significantly enhances reliability in low-quality datasets, as indicated by a high probability of bias factors.

Our approach outperformed the maximum method with mean field bias correction. The most substantial improvements were observed with heavy rainfall estimates in radar signal-blocked regions. The proposed technique provides a robust solution for generating high-quality radar-rainfall time series and real-time assessments. Extending radar compositing to larger areas is feasible with multiple radar stations. The approach relies on radar reflectivity and a dynamic QI, derived from radar-specific factors and computed hourly, making it adaptable to various operational settings. Scaling up bias adjustment using localized QI thresholds improves accuracy and spatial consistency. In areas with dense rain gauge networks, incorporating multiple QI categories allows for finer-scale corrections, with thresholds optimized for each region. Incorporating QI as a weighting factor in spatially distributed bias correction (SDBC) may further enhance bias adjustment accuracy in areas with heterogeneous radar performance. However, this approach requires denser rain gauge networks and increased computational resources compared to the MFB method. Despite these challenges, the application of SDBC in real-time operations may be feasible and warrants further investigation.

Integrating our refined radar quality index-based bias correction with spatially distributed hydrological modeling offers a promising methodology to enhance the accuracy of flood hydrograph prediction and strengthen near real-time flash flood and landslide early warning systems in mountainous terrains. Furthermore, radar rainfall nowcasting could further extend lead times of the early warning system by assuming stable QI factors from the previous hour.

CRediT authorship contribution statement

Monton Methaprayun: Writing – original draft, Visualization, Validation, Software, Investigation, Formal analysis. **Thom Bogaard:** Writing – review & editing, Visualization, Validation, Supervision, Resources, Project administration, Investigation, Conceptualization. **Punpim Puttaraksa Mapiam:** Writing – review & editing, Writing – original draft, Visualization, Validation, Supervision, Resources, Project administration, Methodology, Investigation, Funding acquisition, Conceptualization.

Declaration of competing interest

The authors declare that they have no known competing financial interests or personal relationships that could have appeared to influence the work reported in this paper.

Acknowledgements

This work was undertaken within the frame- work of a research exchange between Kasetsart University (KU), Thailand, and Delft University of Technology (TU Delft), the Netherlands. The authors

gratefully acknowledge the Faculty of Engineering at KU [grant numbers 66/05/WE/D.Eng] and The Capacity Building of KU Students on Internationalization Program (KUCSI) from The International Affairs Division, KU [grant numbers KUCSI221615F7] for financially supporting this research, including Monton Methaprayun's 6-month guest visit to TU Delft, and Thom Bogaard's 2-month guest visit to KU. We also extend our appreciation to the Agricultural Research Development Agency (Public Organization) [grant number PRP6605030140]. for project funding. The authors wish to thank the Department of Royal Rainmaking and Agricultural Aviation (DRRAA) for providing the radar reflectivity data, and the Hydro-Informatics Institute (HII) and the Department of Water Resources (DWR), Thailand, for providing rain gauge data used in this study. Finally, the authors would like to express our appreciation to Prof. Dr. Ir. Remko Uijlenhoet for his constructive comments, which contributed to the improvement of the paper.

Appendix A:. Radar data and quality control

The radar reflectivity products of the Sattahip and Phimai radars are provided on a Cartesian grid covering a 240 × 240 km^2 extent with a 0.6 × 0.6 km^2 spatial resolution and a 6-minute temporal resolution. Both radars provide reflectivity data derived from the 2.5 km pseudo-CAPPI. The radars have different properties, as listed in Table A1.

Table A1
Specification of the Sattahip and Phimai weather radars.

Parameter	Sattahip radar	Phimai radar
Radar type	Doppler S-band	Doppler S-band
Location	12.649° N, 100.963° E	15.182° N, 102.564° E
Height of the radar antenna above mean sea level (m)	174	220
Frequency (GHz)	2.86	2.8
Pulse width (μs)	0.8	0.8
Beam width (°)	1.0	1.2
Wavelength (cm)	10.45	10.70
Peak transmitted power (kW)	927	850
Measurement radius (km)	240	240
CAPPI range (km)	7–139	6–136
CAPPI height (km)	2.5	2.5
Temporal resolution (min)	6	6
Spatial resolution (m)	600 × 600	600 × 600
Tilt angles (°)	0.5, 1.5, 2.4, 3.4, 4.3, 5.3, 6.2, 7.5, 8.7, 10.0, 12.0, 14.0, 16.7, 19.5	0.5, 1.7, 2.5, 3.4, 4.2, 5.1, 6.0, 7.4, 9.2, 11.6, 14.8, 18.4, 22.0

To investigate the effect of different hardware characteristics on reflectivity measurement, radar reflectivity data from overlapping areas observed by both radars within equidistant zones (Keem et al., 2019) were compared across 51 heavy rainfall events from 2016 to 2022, as shown in Fig. A1. The results indicate that the Sattahip radar consistently reports higher reflectivity values than the Phimai radar. This systematic bias suggests that hardware performance likely contributes to the observed discrepancies between the two datasets.

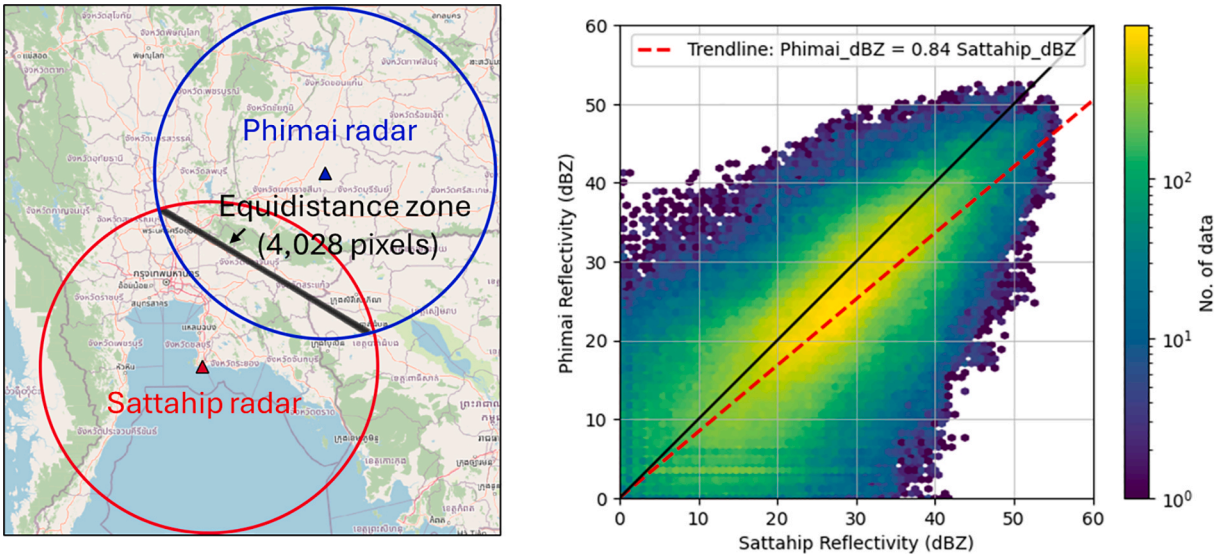

Fig. A1. Scatter plot of radar reflectivity measurements from Sattahip and Phimai radars within the equidistant zones.

Attenuation is considered a significant issue for X-band and C-band radars, particularly in the measurement of high-intensity rainfall (reflectivity > 50 dBZ; Hildebrand, 1978; Austin, 1987; Gu et al., 2011). While beam attenuation is generally assumed to be negligible for S-band radars (Hitschfeld and Bordan, 1954; Delrieu et al., 2000), it can still become relevant during intense precipitation events (Seo et al., 2020). The impact of attenuation can be assessed by examining the relationship between gauge and radar rainfall as a function of distance from the radar (Burrows and Attwood, 1949).

In this study, we investigated the effect of attenuation on individual radars by analyzing the hourly bias factor (G/R ratio) at rain gauge locations as a function of radar distance using 51 heavy rainfall events from 2016 to 2022. The Z–R relationship, $Z = 200R^{1.6}$, proposed by Marshall and Palmer (1948), was applied for radar rainfall estimation for both radars. The results, presented in Fig. A2, show some variation in the bias factor depending on rain gauge location, with relatively few gauges located within 100 km of the radar. However, the bias factor remains generally consistent across different range intervals. This confirms that attenuation effect can be considered negligible for the S-band radars at Sattahip and Phimai.

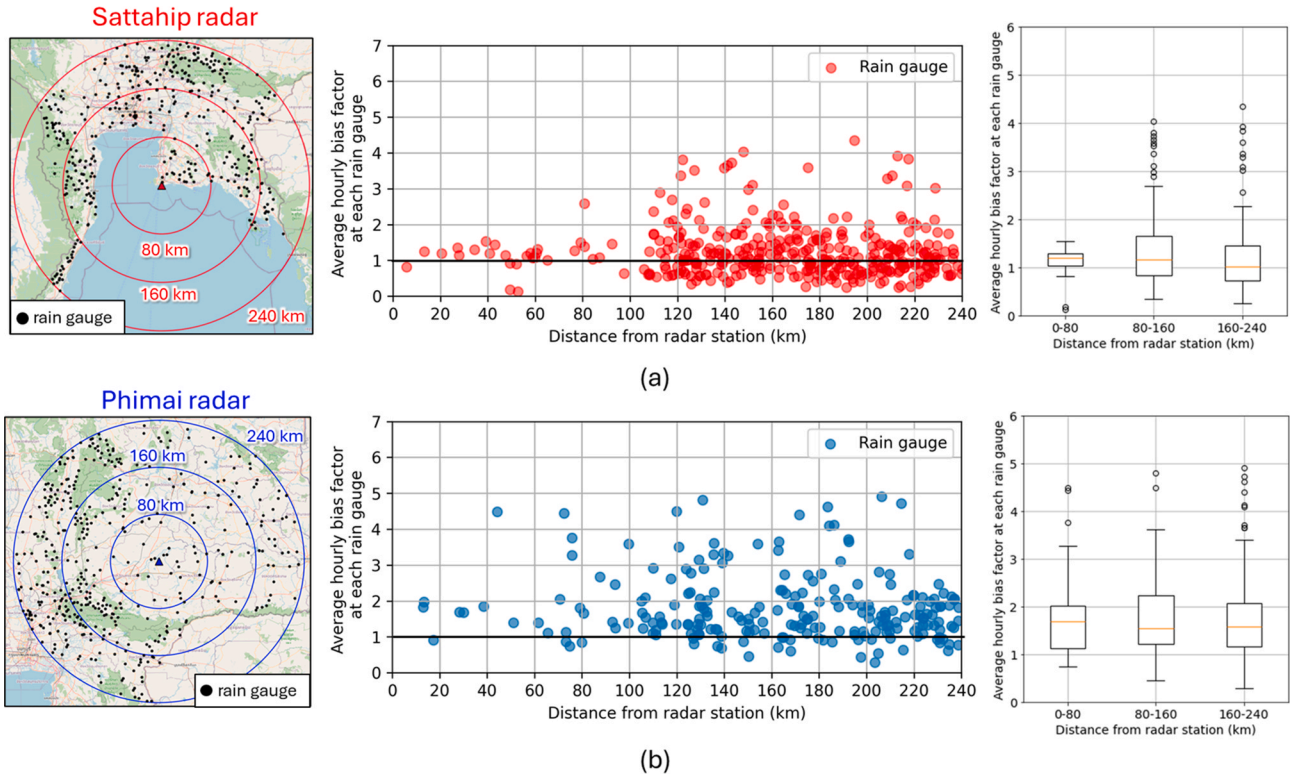

Fig. A2. Mean hourly bias factor at individual rain gauges as a function of range from radar: (a) Sattahip radar, (b) Phimai radar.

The altitude of the freezing level in Thailand is approximately 4.9–5.5 km (Silverman and Sukarnjanaset, 2000). Based on the beam propagation equation proposed by Doviak and Zrnić (1993), the maximum radar range for the Sattahip and Phimai stations at which the upper edge of the radar beam remains below the freezing level of 4.9 km is approximately 170 km. Beyond this range, radar observations are likely to be affected by bright band contamination. Due to limited access to volume scan data, the bright band effect on radar products was investigated using an objective identification method proposed by Cheng and Collier (1993). This approach analyzes the relationship between area-average rainfall rate and the fractional area exceeding specified rainfall thresholds. Bright band contamination is indicated by outliers in this relationship, where rainfall rates are abnormally high relative to the corresponding fractional coverage. Radar reflectivity data from Sattahip and Phimai stations (90–240 km range) were collected for 51 heavy rainfall events (2016–2022) and converted to rainfall rates using the Z-R relationship $Z = 200R^{1.6}$ (Marshall and Palmer, 1948). For each time step, the area-averaged rainfall rate and the fractional area exceeding the 0.5 mm/h and 1 mm/h thresholds were computed. The results presented in Fig. A3 reveal that data points closely follow the regression lines for both thresholds, with no substantial outliers observed, suggesting that bright band contamination in the radar measurements is negligible.

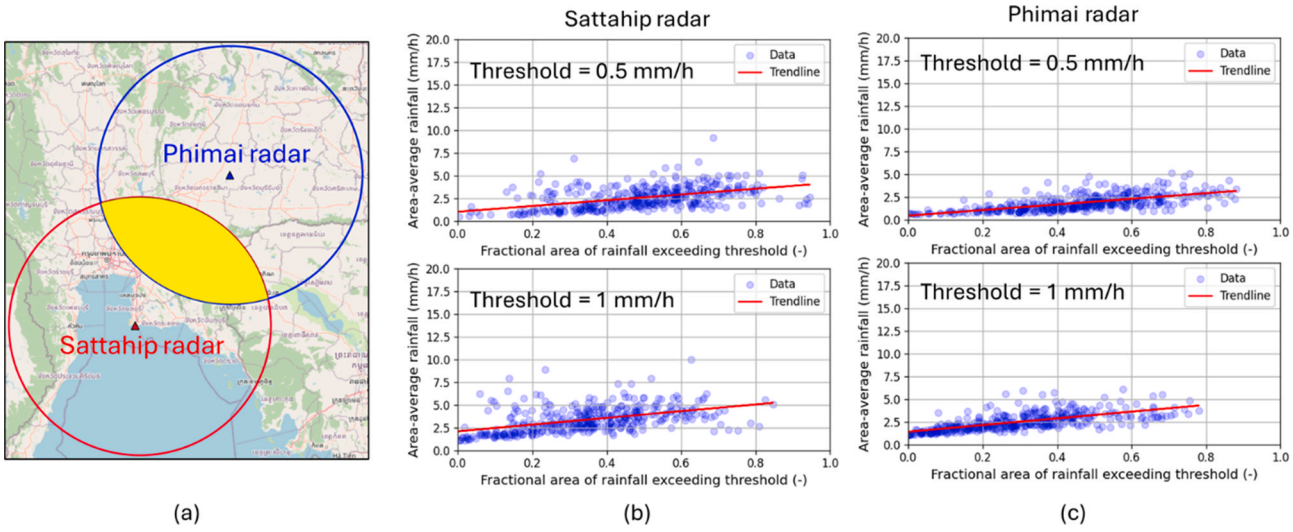

Fig. A3. (a) Radar coverage areas for the Sattahip and Phimai radars (each with a 240 km radius) and their overlapping composite area. (b, c) Scatter plots showing the relationship between area-average rainfall rates and the fractional area exceeding rainfall thresholds of 0.5 mm/h and 1 mm/h during 51 rainfall events (2016–2022), based on radar data within the composite area: (b) Sattahip radar and (c) Phimai radar.

The results presented in Fig. A4 show a comparison between the original radar image and the image after applying the 15 dBZ threshold for the Phimai radar on 2nd October 2020 at 17:00 UTC.

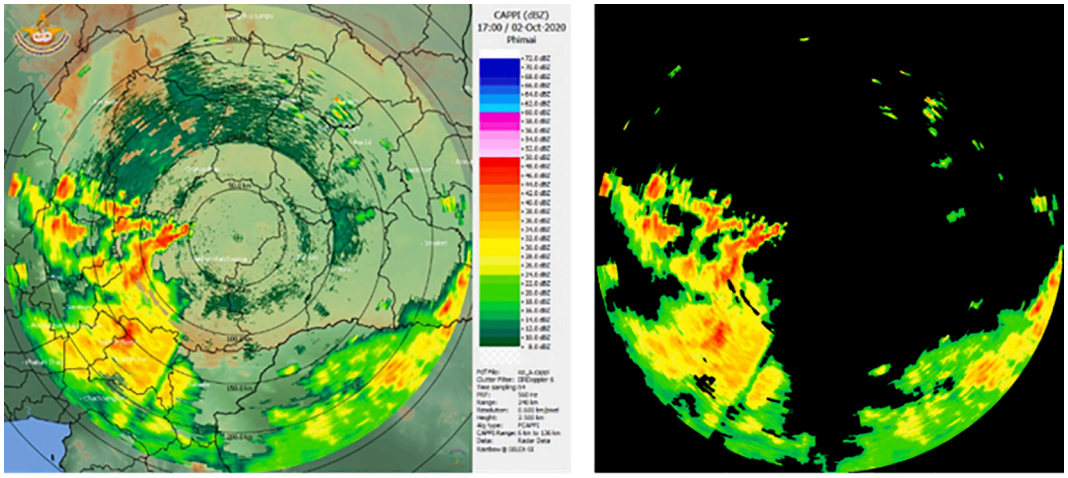

Fig. A4. Reflectivity data from the Phimai radar on 2nd October 2020 at 17:00 UTC: (a) before and (b) after applying a 15 dBZ threshold filter to remove low-intensity, non-precipitating echoes.

Appendix B:. Qualitative comparison of R_{MAX} and RQI_{DHBF} composite products based on the smoothness index

For clarity, radar composite for four storm events are presented in Fig. B1. In all events, the R_{MAX} method often exhibits inconsistencies along the edges of the composite area, where storm structures from adjacent radars fail to align seamlessly. On the other hand, RQI_{DHBF} mitigates measurement inconsistencies, resulting in more coherent and continuous storm representations. When the differences along radar boundaries are minimal, both compositing methods tend to produce similar smoothness values with smaller percentage differences, as observed in Event 21 and 18. However, for Event 4, 31 and 42, where more severe discontinuities in storm patterns occur along radar edges, the differences in smoothness values become more pronounced. The larger percentage differences in these cases reflect degraded storm structure consistency in the R_{MAX} composites. These results suggest that smoothness is a useful indicator for evaluating the spatial coherence and quality of radar rainfall composites.

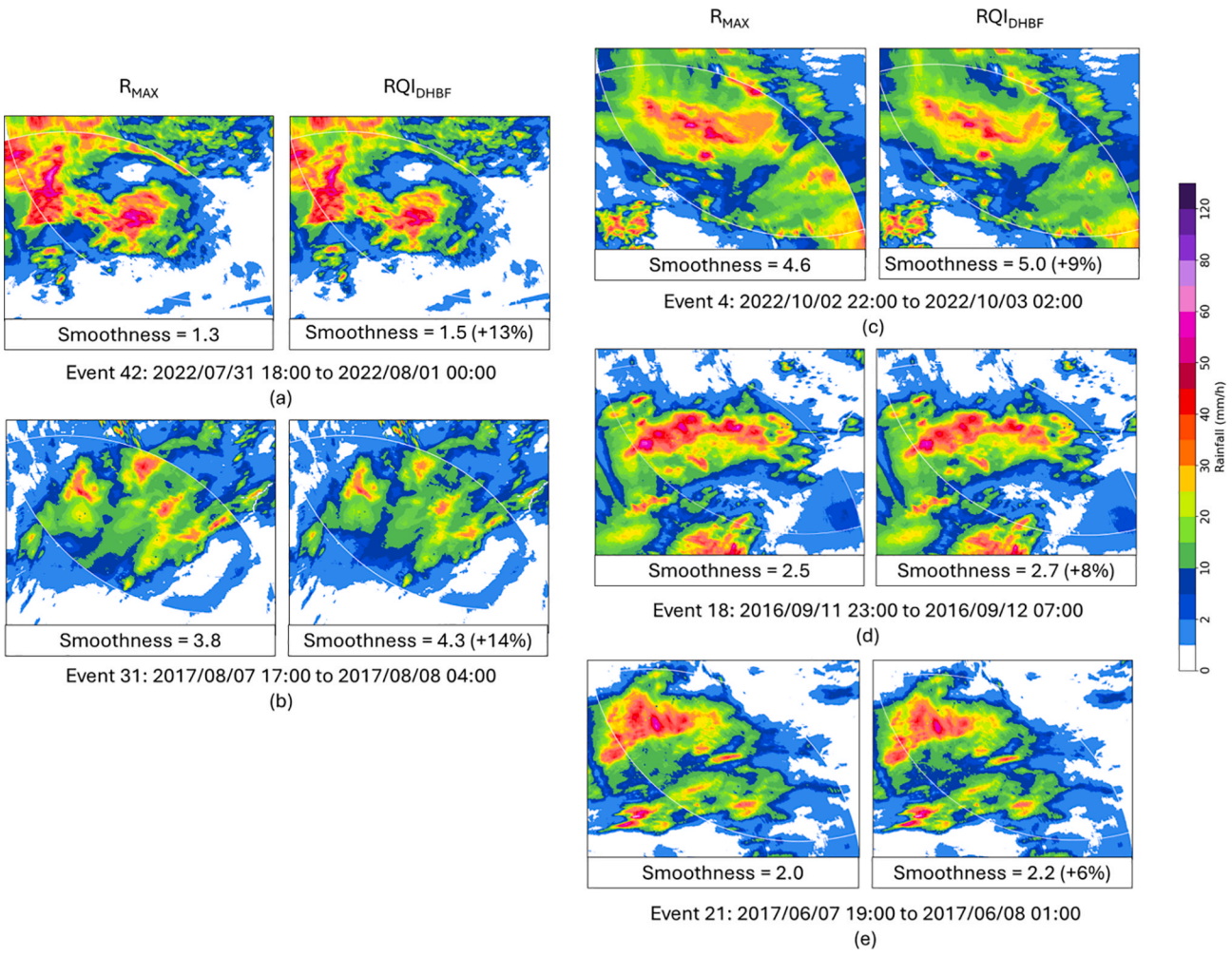

Fig. B1. Comparison of event-based smoothness index comparison between the composite methods R_{MAX} and RQI_{DHBF} for different events (percent improvement shown in parentheses): (a) from July 31, 2022 at 18:00 to August 1, 2022 at 00:00 LST, (b) from August 7, 2017 at 17:00 to August 08, 2017 at 04:00 LST, (c) from October 2, 2022 at 22:00 to October 3, 2022 at 02:00 LST, (d) from September 11, 2016 at 23:00 to September 12, 2016 at 07:00 LST, (e) from June 7, 2017 at 19:00 to June 8, 2017 at 01:00 LST.

Appendix C:. The influence of rain gauge network density on the uncertainty of radar rainfall estimates

In Case 4, the RQI_{DHBF} – MFB_{QI} method exhibits the widest uncertainty in the RMSE. However, it still manages to improve the RMSE by 61 % to 11.7 % for the lower 25th percentile and the upper 75th percentile, respectively, compared with the R_{MAX} – MFB. These findings in Case 4 highlight the influence of the density limitation of the rain gauge networks available on the performance and uncertainty of radar rainfall estimates (Mapiam et al, 2022). The R_{MAX} – MFB method used all rain gauges with heavy rainfall within the composite area to analyze mean field bias factors, whereas the RQI_{DHBF} – MFB_{QI} method utilizes only rain gauges with heavy rainfall and located in regions of poor-quality radar data. This difference in approach contributes to greater uncertainty in the RQI_{DHBF} – MFB_{QI} method compared to the R_{MAX} – MFB.

Fig. C1 illustrates two events showcasing the uncertainty in radar rainfall estimates influenced by the density of rain gauge networks used for bias factor calculations. For the assessment of Case 4, it demonstrates that during Event (a) (August 27, 2022, from 21:00 to 22:00 LST), there were 7 and 20 rain gauges available for calculating the RQI_{DHBF} – MFB_{QI} and R_{MAX} – MFB, respectively. On the other hand, during Event (b) (September 9, 2020, from 13:00 to 14:00 LST), these numbers were 1 and 8, respectively. Comparing the RQI_{DHBF} – MFB_{QI} with the R_{MAX} – MFB approach, it is evident that the former significantly improves the RMSE for Event (a), reflecting the dense rain gauge density accessibility. However, in cases like Event (b), where the rain gauge density is low with only 1 station available, the RQI_{DHBF} – MFB_{QI} could lead to weaker RMSE compared to R_{MAX} – MFB. Moreover, the uncertainty in the RMSE obtained from the RQI_{DHBF} – MFB_{QI} is notably higher than that obtained from the R_{MAX} – MFB technique.

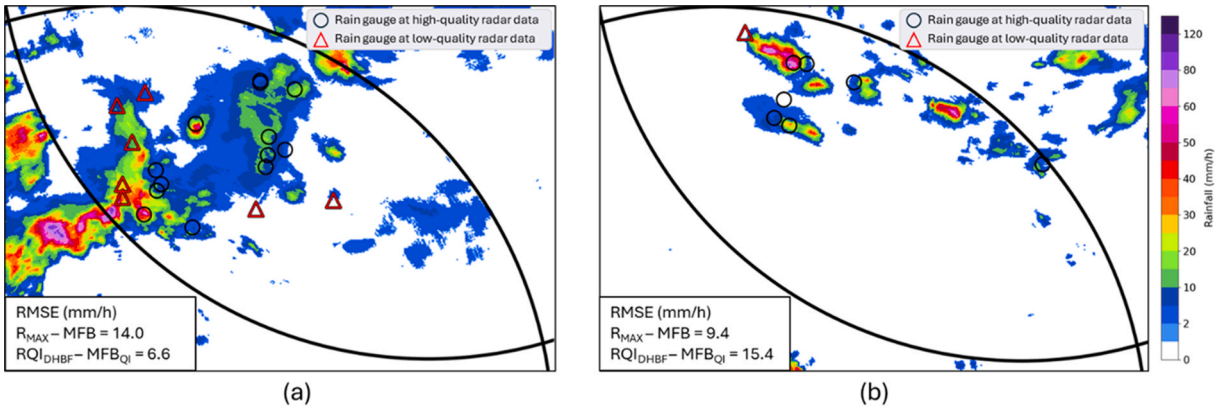

Fig. C1. Example of two events showcasing the uncertainty in radar rainfall estimates influenced by the density of rain gauge networks used for bias factor calculations for Event (a) on August 20, 2022, from 21:00 to 22:00 LST, and Event (b) on September 3, 2020, from 13:00 to 14:00 LST.

Data availability

Data will be made available on request.

References

Antonini, A., Melani, S., Corongiu, M., Romanelli, S., Mazza, A., Ortolani, A., Gozzini, B., 2017. On the implementation of a regional X-band weather radar network. Atmos. 8, 25. https://doi.org/10.3390/atmos8020025.

Atlas, D., 2002. Radar calibration: some simple approaches. Bull. Am. Meteorol. Soc. 83 (9), 1313–1316. https://doi.org/10.1175/1520-0477-83.9.1313.

Austin, P.M., 1987. Relation between measured radar reflectivity and surface rainfall. Mon. Weather Rev. 115 (5), 1053–1070. https://doi.org/10.1175/1520-0493(1987)115<1053:RBMRRA>2.0.CO;2.

Barbieri, S., Di Fabio, S., Lidori, R., Rossi, F.L., Marzano, F.S., Picciotti, E., 2022. Mosaicking weather radar retrievals from an operational heterogeneous network at C and X band for precipitation monitoring in italian central apennines. Remote Sens. (Basel) 14, 248. https://doi.org/10.3390/rs14020248.

Bárdossy, A., Pegram, G., 2017. Combination of radar and daily precipitation data to estimate meaningful sub-daily point precipitation extremes. J. Hydrol. 544, 397–406. https://doi.org/10.1016/j.jhydrol.2016.11.039.

Bech, J., Codina, B., Lorente, J., Bebbington, D., 2003. The sensitivity of single polarization weather radar beam blockage correction to variability in the vertical refractivity gradient. J. Atmos. Oceanic Tech. 20, 845–855. https://doi.org/10.1175/1520-0426(2003)020<0845:TSOSPW>2.0.CO;2.

Bech, J., Gjertsen, U., Haase, G., 2007. Modelling weather radar beam propagation and topographical blockage at northern high latitudes. Q. J. R. Meteorolog. Soc. 133, 1191–1204. https://doi.org/10.1002/qj.98.

Bogaard, T., Greco, R., 2018. Invited perspectives: Hydrological perspectives on precipitation intensity-duration thresholds for landslide initiation: proposing hydro-meteorological thresholds. Nat. Hazards Earth Syst. Sci. 18, 31–39. https://doi.org/10.5194/nhess-18-31-2018.

Burrows, D.R., Attwood, S.S., 1949. Radio Wave Propagation. Academic Press, p. 219.

Chen, H., Cifelli, R., Chandrasekar, V., Ma, Y., 2019. A flexible bayesian approach to bias correction of radar-derived precipitation estimates over complex terrain: model design and initial verification. J. Hydrometeorol. 20 (12), 2367–2382. https://doi.org/10.1175/JHM-D-19-0136.1.

Cheng, M., Collier, C.G., 1993. An objective method for recognizing and partially correcting brightband error in radar images. J. Appl. Meteorol. (1988–2005), 32(6), 1142–1149, doi: 10.1175/1520-0450(1993)032<1142:AOMFRA>2.0.CO;2.

Chumchean, S., Seed, A., Sharma, A., 2006. Correcting of real-time radar rainfall bias using a Kalman filtering approach. J. Hydrol. 317 (1), 123–137. https://doi.org/10.1016/j.jhydrol.2005.05.013.

Cole, S.J., Moore, R.J., 2008. Hydrological modelling using raingauge- and radar-based estimators of areal rainfall. J. Hydrol. 358, 159–181. https://doi.org/10.1016/j.jhydrol.2008.05.025.

Creutin, J.D., Borga, M., 2003. Radar hydrology modifies the monitoring of flash-flood hazard. Hydrol. Process. 17. https://doi.org/10.1002/hyp.5122.

Crisologo, I., Warren, R.A., Mühlbauer, K., Heistermann, M., 2018. Enhancing the consistency of spaceborne and ground-based radar comparisons by using beam blockage fraction as a quality filter. Atmos. Meas. Tech. 11, 5223–5236. https://doi.org/10.5194/amt-11-5223-2018.

Delrieu, G., Andrieu, H., Creutin, J.D., 2000. Quantification of path-integrated attenuation for X- and C-band weather radar systems operating in Mediterranean heavy rainfall. J. Appl. Meteorol. 39 (6), 840–850. https://doi.org/10.1175/1520-0450(2000)039<0840:QOPIAF>2.0.CO;2.

Doviak, R.J., Zrnić, D.S., 1993. Precipitation measurements. In: Doviak, R.J., Zrnić, D.S. (Eds.), Doppler Radar and Weather Observations (Second Edition). Academic Press, San Diego, pp. 209–279. https://doi.org/10.1016/B978-0-12-221422-6.50013-9.

Dufton, D.R.L., Collier, C.G., 2015. Fuzzy logic filtering of radar reflectivity to remove non-meteorological echoes using dual polarization radar moments. Atmos. Meas. Tech. 8 (10), 3985–4000. https://doi.org/10.5194/amt-8-3985-2015.

Einfalt, T., Lobbrecht, A., 2012. Compositing international radar data using a weight-based scheme. IAHS AISH Publ. 20–25.

Fornasiero, A., Bech, J., Alberoni, P.P., 2006. Enhanced radar precipitation estimates using a combined clutter and beam blockage correction technique. Nat. Hazards Earth Syst. Sci. 6, 697–710. https://doi.org/10.5194/nhess-6-697-2006.

Fulton, R.A., Breidenbach, J.P., Seo, D.-J., Miller, D.A., O'Bannon, T., 1998. The WSR-88D rainfall algorithm. Weather Forecast. 13, 377–395. https://doi.org/10.1175/1520-0434(1998)013<0377:TWRA>2.0.CO;2.

Gu, J.-Y., Ryzhkov, A., Zhang, P., Neilley, P., Knight, M., Wolf, B., Lee, D.-I., 2011. Polarimetric attenuation correction in heavy rain at C band. J. Appl. Meteorol. Climatol. 50 (1), 39–58. https://doi.org/10.1175/2010JAMC2258.1.

Guzzetti, F., Peruccacci, S., Rossi, M., Stark, C.P., 2007. Rainfall thresholds for the initiation of landslides in central and southern Europe. Meteorol. Atmos. Phys. 98, 239–267. https://doi.org/10.1007/s00703-007-0262-7.

Harrison, D.L., Scovell, R.W., Kitchen, M., 2009. High-resolution precipitation estimates for hydrological uses. Proc. Inst. Civil Eng. - Water Manage. 162, 125–135. https://doi.org/10.1680/wama.2009.162.2.125.

Hazenberg, P., Torfs, P.J.J.F., Leijnse, H., Delrieu, G., Uijlenhoet, R., 2013. Identification and uncertainty estimation of vertical reflectivity profiles using a Lagrangian approach to support quantitative precipitation measurements by weather radar, 10243–210261 J. Geophys. Res. Atmos. 118 (18). https://doi.org/10.1002/jgrd.50726.

Hildebrand, P.H., 1978. Iterative correction for attenuation of 5 cm radar in rain. J. Appl. Meteorol. Climatol. 17 (4), 508–514. https://doi.org/10.1175/1520-0450(1978)017<0508:ICFAOC>2.0.CO;2.

Hitschfeld, W., Bordan, J., 1954. Errors inherent in the radar measurement of rainfall at attenuating wavelengths. J. Atmos. Sci. 11 (1), 58–67. https://doi.org/10.1175/1520-0469(1954)011<0058:EIITRM>2.0.CO;2.

Holleman, I., 2007. Bias adjustment and long-term verification of radar-based precipitation estimates. Meteorol. Appl. 14, 195–203. https://doi.org/10.1002/met.22.

Imhoff, R., Brauer, C., van Heeringen, K.J., Leijnse, H., Overeem, A., Weerts, A., Uijlenhoet, R., 2021. A climatological benchmark for operational radar rainfall bias reduction. Hydrol. Earth Syst. Sci. 25, 4061–4080. https://doi.org/10.5194/hess-25-4061-2021.

Joss, J., Waldvogel, A., Collier, C.G., 1990. Precipitation Measurement and Hydrology, in: Radar in Meteorology: Battan Memorial and 40th Anniversary Radar Meteorology Conference, edited by: Atlas, D., American Meteorological Society, Boston, MA, 577-606, doi: 10.1007/978-1-935704-15-7_39.

Jurczyk, A., Szturc, J., Ośródka, K., 2020. Quality-based compositing of weather radar derived precipitation. Meteorol. Appl. 27, e1812.

Keem, M., Seo, B.-C., Krajewski, W.F., Morris, K.R., 2019. Inter-comparison of reflectivity measurements between GPM DPR and NEXRAD radars. Atmos. Res. 226, 49–65. https://doi.org/10.1016/j.atmosres.2019.04.010.

Krajewski, W.F., Ntelekos, A.A., Goska, R., 2006. A GIS-based methodology for the assessment of weather radar beam blockage in mountainous regions: two examples from the US NEXRAD network. Comput. Geosci. 32, 283–302. https://doi.org/10.1016/j.cageo.2005.06.024.

Krajewski, W.F., Villarini, G., Smith, J.A., 2010. RADAR-rainfall uncertainties: where are we after thirty years of effort? Bull. Am. Meteorol. Soc. 91, 87–94. https://doi.org/10.1175/2009BAMS2747.1.

Krajewski, W.F., Ceynar, D., Demir, I., Goska, R., Kruger, A., Langel, C., Mantilla, R., Niemeier, J., Quintero, F., Seo, B.-C., Small, S.J., Weber, L.J., Young, N.C., 2017. Real-Time flood forecasting and information system for the state of Iowa. Bull. Am. Meteorol. Soc. 98, 539–554. https://doi.org/10.1175/BAMS-D-15-00243.1.

Kucera, P.A., Krajewski, W.F., Young, C.B., 2004. Radar beam occultation studies using GIS and DEM technology: an example study of Guam. J. Atmos. Oceanic Tech. 21,

995–1006. https://doi.org/10.1175/1520-0426(2004)021<0995:RBOSUG>2.0.CO;2.
Lang, T.J., Nesbitt, S.W., Carey, L.D., 2009. On the correction of partial beam blockage in polarimetric radar data. J. Atmos. Oceanic Tech. 26, 943–957. https://doi.org/10.1175/2008JTECHA1133.1.
Lee, J.-E., Kwon, S., Jung, S.-H., 2021. Real-time calibration and monitoring of radar reflectivity on nationwide dual-polarization weather radar network. Remote Sens. (Basel) 13, 2936. https://doi.org/10.3390/rs13152936.
Mapiam, P.P., Methaprayun, M., Bogaard, T., Schoups, G., Ten Veldhuis, M.C., 2022. Citizen rain gauges improve hourly radar rainfall bias correction using a two-step Kalman filter. Hydrol. Earth Syst. Sci. 26, 775–794. https://doi.org/10.5194/hess-26-775-2022.
Mapiam, P.P., Sakulnurak, S., Methaprayun, M., Makmee, C., Marjang, N., 2023. Downscaling the Z–R relationship and bias correction solution for flash flood assessment in a data-scarce basin, Thailand. Water Sci. Technol. 87, 1259–1272. https://doi.org/10.2166/wst.2023.056.
Marra, F., Morin, E., 2015. Use of radar QPE for the derivation of Intensity–Duration–Frequency curves in a range of climatic regimes. J. Hydrol. 531, 427–440. https://doi.org/10.1016/j.jhydrol.2015.08.064.
Marshall, J.S., Palmer, W.M.K., 1948. The distribution of raindrops with size. J. Atmos. Sci. 5, 165–166. https://doi.org/10.1175/1520-0469(1948)005<0165:TDORWS>2.0.CO;2.
McRoberts, D.B., Nielsen-Gammon, J.W., 2017. Detecting beam blockage in radar-based precipitation estimates. J. Atmos. Oceanic Tech. 34, 1407–1422. https://doi.org/10.1175/JTECH-D-16-0174.1.
Mekonnen, K., Melesse, A.M., Woldesenbet, T.A., 2021. Spatial evaluation of satellite-retrieved extreme rainfall rates in the Upper Awash River Basin, Ethiopia. Atmos. Res. 249, 105297. https://doi.org/10.1016/j.atmosres.2020.105297.
Mesnard, F., Sauvageot, H., 2010. Climatology of anomalous propagation radar echoes in a coastal area. J. Appl. Meteorol. Climatol. 49 (11), 2285–2300. https://doi.org/10.1175/2010JAMC2440.1.
Méri, L., Gaál, L., Bartok, J., Gažák, M., Gera, M., Jurašek, M., Kelemen, M., 2021. Improved radar composites and enhanced value of meteorological radar data using different quality indices. Sustainability 13 (9), 5285. https://doi.org/10.3390/su13095285.
Michelson, D.B., Koistinen, J., 2000. Gauge-Radar network adjustment for the Baltic sea experiment. Phys. Chem. Earth Part B 25, 915–920. https://doi.org/10.1016/S1464-1909(00)00125-8.
Ośródka, K., Szturc, J., Jurczyk, A., 2014. Chain of data quality algorithms for 3-D single-polarization radar reflectivity (RADVOL-QC system). Meteorol. Appl. 21 (2), 256–270. https://doi.org/10.1002/met.1323.
Ośródka, K., Szturc, J., 2015. Quality-based generation of weather radar Cartesian products. Atmos. Meas. Tech. 8 (5), 2173–2181. https://doi.org/10.5194/amt-8-2173-2015.
Ośródka, K., Szturc, J., 2022. Improvement in algorithms for quality control of weather radar data (RADVOL-QC system). Atmos. Meas. Tech. 15 (2), 261–277. https://doi.org/10.5194/amt-15-261-2022.
Overeem, A., van den Besselaar, E., van der Schrier, G., Meirink, J.F., van der Plas, E., Leijnse, H., 2023. EURADCLIM: the European climatological high-resolution gauge-adjusted radar precipitation dataset. Earth Syst. Sci. Data 15, 1441–1464. https://doi.org/10.5194/essd-15-1441-2023.
Pellarin, T., Delrieu, G., Saulnier, G.-M., Andrieu, H., Vignal, B., Creutin, J., 2002. Hydrologic visibility of weather radar systems operating in mountainous regions: case study for the Ardèche Catchment (France). J. Hydrometeorol. 3. https://doi.org/10.1175/1525-7541(2002)003<0539:HVOWRS>2.0.CO;2.
Saltikoff, E., Haase, G., Delobbe, L., Gaussiat, N., Martet, M., Idziorek, D., Leijnse, H., Novák, P., Lukach, M., Stephan, K., 2019. OPERA the Radar Project. Atmos. 10, 320. https://doi.org/10.3390/atmos10060320.
Schleiss, M., Olsson, J., Berg, P., Niemi, T., Kokkonen, T., Thorndahl, S., Nielsen, R., Ellerbæk Nielsen, J., Bozhinova, D., Pulkkinen, S., 2020. The accuracy of weather radar in heavy rain: a comparative study for Denmark, the Netherlands, Finland and Sweden. Hydrol. Earth Syst. Sci. 24, 3157–3188. https://doi.org/10.5194/hess-24-3157-2020.
Searcy, J.K., Hardison, C.H., 1960. Double-mass curves. US Government Printing Office.
Seo, D.J., Breidenbach, J.P., Johnson, E.R., 1999. Real-time estimation of mean field bias in radar rainfall data. J. Hydrol. 223, 131–147. https://doi.org/10.1016/S0022-1694(99)00106-7.
Seo, B.-C., Krajewski, Smith, J.A., 2014. Four-dimensional reflectivity data comparison between two ground-based radars: methodology and statistical analysis. Hydrol. Sci. J. 59 (7), 1320–1334. https://doi.org/10.1080/02626667.2013.839872.
Seo, B.-C., Krajewski, W.F., Ryzhkov, A., 2020. Evaluation of the specific attenuation method for radar-based quantitative precipitation estimation: improvements and practical challenges. J. Hydrometeorol. 21 (6), 1333–1347. https://doi.org/10.1175/JHM-D-20-0030.1.
Shi, Z., Wei, F., Chandrasekar, V., 2018. Radar-based quantitative precipitation estimation for the identification of debris flow occurrence over earthquake-affected regions in Sichuan, China. Nat. Hazards Earth Syst. Sci. 18, 765–780. https://doi.org/10.5194/nhess-18-765-2018.
Silverman, B.A., Sukarnjanaset, W., 2000. Results of the thailand warm-cloud hygroscopic particle seeding experiment. J. Appl. Meteorol. 39 (7), 1160–1175. https://doi.org/10.1175/1520-0450(2000)039<1160:ROTTWC>2.0.CO;2.
Smith, J.A., Krajewski, W.F., 1991. Estimation of the mean field bias of radar rainfall estimates. J. Appl. Meteorol. Climatol. 30, 397–412. https://doi.org/10.1175/1520-0450(1991)030<0397:Eotmfb>2.0.Co;2.
Steiner, M., Smith, J.A., Burges, S.J., Alonso, C.V., Darden, R.W., 1999. Effect of bias adjustment and rain gauge data quality control on radar rainfall estimation. Water Resour. Res. 35, 2487–2503. https://doi.org/10.1029/1999WR900142.
Szturc, J., Ośródka, K., Jurczyk, A., 2011. Quality index scheme for quantitative uncertainty characterization of radar-based precipitation. Meteorol. Appl. 18, 407–420. https://doi.org/10.1002/met.230.
Tabary, P., 2007. The new French operational radar rainfall product Part I: methodology. Weather Forecast. 22, 393–408. https://doi.org/10.1175/WAF1004.1.
Thorndahl, S., Nielsen, J.E., Rasmussen, M.R., 2014. Bias adjustment and advection interpolation of long-term high resolution radar rainfall series. J. Hydrol. 508, 214–226. https://doi.org/10.1016/j.jhydrol.2013.10.056.
Uijlenhoet, R., 2001. Raindrop size distributions and radar reflectivity–rain rate relationships for radar hydrology. Hydrol. Earth Syst. Sci. 5 (4), 615–628. https://doi.org/10.5194/hess-5-615-2001.
Uijlenhoet, R., Berne, A., 2008. Stochastic simulation experiment to assess radar rainfall retrieval uncertainties associated with attenuation and its correction. Hydrol. Earth Syst. Sci. 12 (2), 587–601. https://doi.org/10.5194/hess-12-587-2008.
Villarini, G., Krajewski, W.F., 2010. Sensitivity studies of the models of radar-rainfall uncertainties. J. Appl. Meteorol. Climatol. 49, 288–309. https://doi.org/10.1175/2009JAMC2188.1.
Warren, R.A., Protat, A., Siems, S.T., Ramsay, H.A., Louf, V., Manton, M.J., Kane, T.A., 2018. Calibrating ground-based radars against TRMM and GPM. J. Atmos. Oceanic Tech. 35 (2), 323–346. https://doi.org/10.1175/JTECH-D-17-0128.1.
Wright, D.B., Smith, J.A., Villarini, G., Baeck, M.L., 2013. Estimating the frequency of extreme rainfall using weather radar and stochastic storm transposition. J. Hydrol. 488, 150–165. https://doi.org/10.1016/j.jhydrol.2013.03.003.
Wright, D.B., Smith, J.A., Villarini, G., Baeck, M.L., 2014. Long-term high-resolution radar rainfall fields for urban hydrology. JAWRA J. Am. Water Resour. Assoc. 50 (3), 713–734. https://doi.org/10.1111/jawr.12139.
Yoo, C., Park, C., Yoon, J., Kim, J., 2014. Interpretation of mean-field bias correction of radar rain rate using the concept of linear regression. Hydrol. Process. 28, 5081–5092. https://doi.org/10.1002/hyp.9972.
Zhang, Y., Liu, L., Wen, H., Yu, B., Wang, H., Zhang, Y., 2022. Combined radar quality index for quantitative precipitation estimation of heavy rainfall events. Remote Sens. https://doi.org/10.3390/rs14133154.
Zhong, L., Yang, R., Wen, Y., Chen, L., Gou, Y., Li, R., Zhou, Q., Hong, Y., 2017. Cross-evaluation of reflectivity from the space-borne precipitation radar and multi-type ground-based weather radar network in China. Atmos. Res. 196, 200–210. https://doi.org/10.1016/j.atmosres.2017.06.016.